Ore Geology Reviews 67 (2015) 314–335

Contents lists available at ScienceDirect

Ore Geology Reviews

journal homepage: www.elsevier.com/locate/oregeorev

The Paleoproterozoic Montviel carbonatite-hosted REE–Nb deposit, Abitibi, Canada: Geology, mineralogy, geochemistry and genesis

Olivier Nadeau [a,b,*], A. Cayer [c], M. Pelletier [c], R. Stevenson [a,b], M. Jébrak [a]

[a] Université du Québec à Montréal, Montreal, Canada
[b] Geotop Research Centre in Geochemistry and Geodynamics, Montreal, Canada
[c] Ressources Géoméga, St-Lambert, Canada

ARTICLE INFO

Article history:
Received 26 September 2014
Received in revised form 15 December 2014
Accepted 18 December 2014
Available online 28 December 2014

Keywords:
Carbonatite-hosted REE and Nb deposits
Magmatic and carbo-hydrothermal processes
Carbonatites

ABSTRACT

The Montviel 250 Mt carbonatite-hosted REE–Nb deposit is hosted in a Paleoproterozoic alkaline suite located in the Sub-Province of Abitibi, in the Archean Province of the Superior. The alkaline intrusion consists of biotite clinopyroxenites, melano- to leucosyenites, a melteigite–ijolite–urtite series, riebeckite granite, a series of carbonatites and a carbonatite polygenic breccia. The carbonatite series includes silicocarbonatites, calciocarbonatites, rare magnesiocarbonatites, ferrocarbonatites and mixed carbonatites and are cut by a late, high-energy carbonatite polygenic breccia. Diamond drill hole assays and microscope observations indicate that Nb is hosted in pyrochlore from silicocarbonatite whereas the REE mineralization is mainly hosted in ferrocarbonatite, late mixed carbonatites and polygenic breccia, in REE-bearing carbonates and fluorocarbonate minerals. Diamond drill hole underground mapping and systematic assays have shed light on zones enriched in Nd and LREE with preferential Ba and Sr hydrothermal precipitation and zones enriched in Dy, Y and HREE displaying preferential F and P bearing hydrothermal precipitation. Petrographic observations, electron microprobe analyses, LA-ICPMS and X-ray diffraction were used to study the mineralization processes and to identify and quantify the REE-bearing burbankite–(Ce), carbocernaite–(Ce), ewaldite–(Y), huanghoite–(Nd), cordylite–(Ce), cordylite–(Nd), kukharenkoite–(Ce) and synchysite–(Ce). Most minerals are enriched in total LREE with values around 19.3 wt.%, have total MREE values around 2.2 wt.% and extremely variable total HREE values, with very high contents of Dy and Y averaging around 0.3 wt.% and 1.0 wt.%, respectively, and with total HREE reaching up to 10.0 wt.%. A paragenetic sequence is proposed that consists of: (1) a silicocarbonatite Nb stage, and (2) a calciocarbonatite stage, dominated by magmatism but accompanied by hydrothermal fluids, (3) a main ferrocarbonatite stage, dominated by episodes of Ba- and Sr-hydrothermalism and LREE mineralization, F- and P-hydrothermalism and HREE mineralization and evolved ferrocarbonatitic magmatism, (4) a renewed, mixed carbonatite magmatic stage with minor but increasing hydrothermalism, and (5) a terminal stage of fluid pressure buildup and explosion, leading to the creation of a HREE-enriched polygenic breccia. Globular melt inclusions of Ba–Cl–F (±Si–O) may indicate the presence and contribution of barium-bearing chlorofluoride melts during hydrothermal activity and mineralization of the carbonatite.

1. Introduction

1.1. Rare earth element deposits

Five metals have been labeled 'critical' for the low-carbon energy sector by the European Commission, two of which are REE: Nd and Dy. Furthermore, out of the 16 rare earth elements (the 14 lanthanides plus Group III Y and Sc), 5 were declared to be economically critical by the US Federal Administration and include Nd, Eu, Tb, Dy and Y. Hence, not all REE are equivalent and the size of REE deposits should not be blindly considered without also taking into account which of the REE are economically enriched. For example, Bayan Obo, in China, is the world's largest REE deposit (48 Mt at 6 wt.% REE_2O_3; Chao et al., 1997) and is hosted by dolomites and carbonatites (Philpotts et al., 1991; Le Bas et al, 1992; Chao et al., 1997; Kynicky et al., 2012; Sun et al., 2013). However, Bayan Obo hosts significantly less critical REE than the South China ion adsorption clays (world's leader in HREE), deposits associated with alkaline granites and pegmatites such as the Strange Lake, Kwyjibo and Nechalacho deposits (Canada), or deposits associated with carbonatites such as the Niobec, Eldor, Montviel, Bear Lodge and Mountain Pass deposits (Canada/USA) (Gauthier et al., 2004; Long et al., 2010; Kynicky et al., 2012; Mariano and Mariano, 2012; Sheard et al., 2012; Quest, Focus Graphite, Avalon, Iamgold, Commerce Resources, Geomega, Rare Element Resources, and Molycorp commercial websites).

* Corresponding author at: Université du Québec à Montréal, Montreal, Canada.

http://dx.doi.org/10.1016/j.oregeorev.2014.12.017
0169-1368/

Most rare earth element (REE) deposits are found in carbonatites, peralkaline granites and pegmatites, and peralkaline, Si-undersaturated feldspathoidal rocks. Carbonatite-hosted REE deposits typically are enriched in light REE (LREE) whereas siliceous REE deposits are more inclined to contain abnormally high levels of heavy REE (HREE) (Chakhmouradian and Zaitsev, 2012). Nevertheless, some HREE-enriched carbonatites exist such as the Lofdal carbonatite, Namibia, where HREE are hosted primarily in xenotime–(Y) (Wall et al., 2008). Carbonates of the mckelveyite group such as mckelveyite and ewaldite–(Y) are also recognized to possibly host HREEs (Chakhmouradian and Zaitsev, 2012).

The mechanisms of REE concentration in carbonatites are diverse. The origin of REE mineralization can be magmatic, hydrothermal, supergene or a combination of these. Most carbonatites experience hydrothermal alteration and carbonatites rarely host solely magmatic REE mineralization. The only example of magmatic carbonatite REE mineralization known to date is that of Mountain Pass carbonatite, USA (Mariano and Mariano, 2012). In general, the more evolved the carbonatite, the greater the hydrothermal mineralization and the greater the total REE concentration (Wall and Mariano, 1996). Hydrothermal REE mineralization may originate from very proximal magmatic sources and have experienced only minor remobilization, with or without magmatic remnants, or hydrothermal fluids may have carried REE elements over longer distances, giving the deposits a true, hydrothermal origin (e.g., Mariano, 1989).

Carbonatites usually host the REE in magmatic calcite, apatite, titanite, REE-bearing perovskite (loparite) or burbankite–(Ce), depending on the activity of REE, P, F and CO_2 in the melt, and REE will generally be transferred to REE–Ba–Ca–Sr–Na carbonates and fluorocarbonates such as bastnäsite–(Ce)–(Ce), carbocernaite–(Ce) and cebaite–(Ce) during hydrothermal activity (Mitchell, 1996; Wall and Mariano, 1996; Wyllie et al., 1996; Hedrick et al., 1997). Although rare earth elements bond with SiO_4^{4-}, CO_3^{2-} and F^- in minerals, they are best transported in hydrothermal fluids as chlorides, and probably also as carbonate and bicarbonate complexes in CO_2-rich fluids (Williams-Jones et al., 2012).

Montviel is an alkaline intrusive suite located in the northeast side of the Abitibi greenstone belt, Canada (Fig. 1). The intrusion consists of a series of biotite clinopyroxenite, melano- to leucosyenites, a suite of melteigite–ijolite–urtite, riebeckite granite, a suite of carbonatites, and a carbonatite polygenic breccia (Fig. 2). The age of the intrusion is constrained by U–Pb zircon dating of an ijolite that yielded an age of 1894 ± 4 Ma (David et al., 2006). It is noteworthy that there are not many 1.9 Ga carbonatites in the world (Woolley and Kjarsgaard, 2008). In Canada there are the Castignon carbonatite, Quebec, and the Borden and Cargill carbonatites, Ontario, which were dated at 1880 ± 2 Ma (Dimroth, 1970), 1872 ± 13 Ma (Bell et al., 1987) and 1907 ± 4 Ma (Sage, 1988), respectively. The present paper focuses on the Montviel carbonatite, a new carbonatite-hosted REE deposit enriched in Nd, Eu, Dy and Y, all of which are critical REEs. The REE mineralization is hosted in Ba–Ca–Sr–Na carbonates and fluorocarbonates, most of which are hydrothermal minerals. It should be noted that hydrothermal fluids at Montviel probably were aqueous and carbonic, like fluids from other carbonatites (e.g., Bühn and Rankin, 1999). Nevertheless, we have adopted the term 'hydrothermal' and avoided the term 'carbo-hydrothermal' to keep the text simpler. The carbonatite is complex and is composed of silicoarbonatite (SiC), calciocarbonatite (CaC), magnesiocarbonatite (MgC), ferrocarbonatite (FeC), mixed SiC–CaC–FeC and a carbonatite polygenic breccia (BXP). In the present paper, the nomenclature of carbonatite follows that previously used in the literature for Montviel (Goutier and Lalonde, 2006a,b; Goutier, 2005) and that based on bulk rock chemistry proposed by Woolley and Kempe (1989). Silicocarbonatite, however, is used for rock with 10 to 50% carbonate minerals.

1.2. History

The Montviel area was first investigated by R. Bell of the Geological Survey of Canada in 1895 and was frequently revisited throughout the 20th century but was not systematically mapped until 1949 by P.E. Imbeault (Desharnais and Duplessis, 2011). The area was first explored

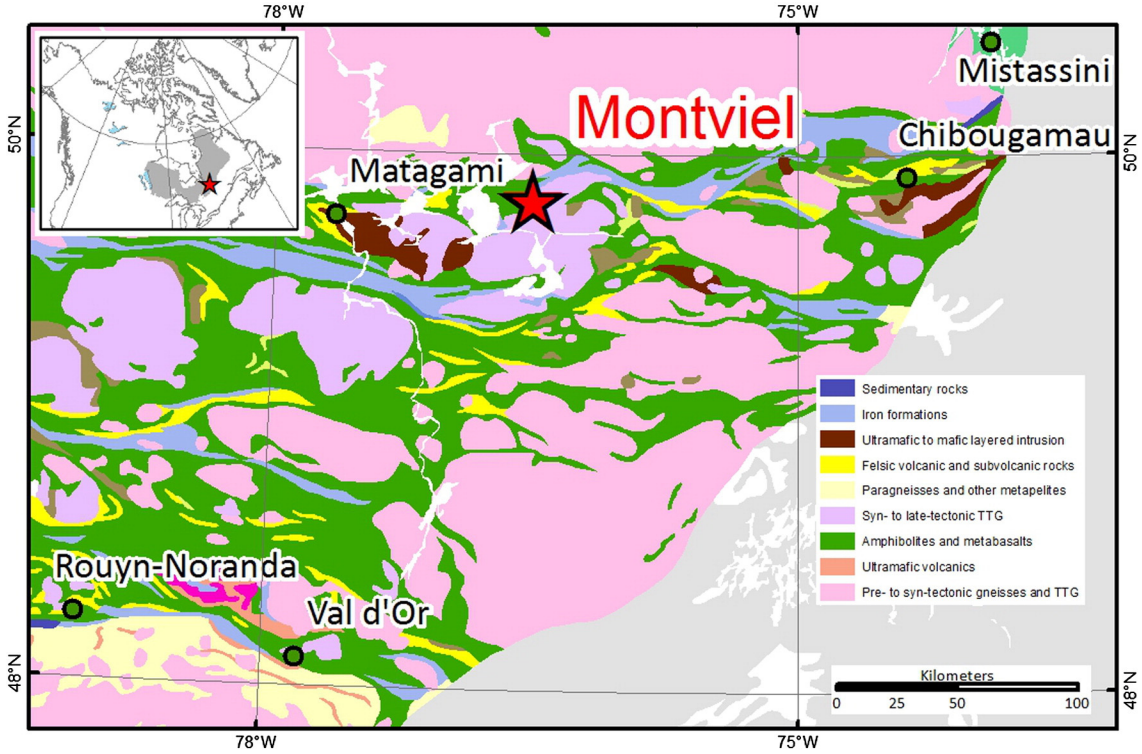

Fig. 1. Regional geological map of Archean East Abitibi showing the location of the Montviel REE–Nb deposit. The undifferentiated Proterozoic Province of Grenville is in gray to the south-east. The geological data is from the Ministère des Ressources Naturelles et de la Faune du Québec.

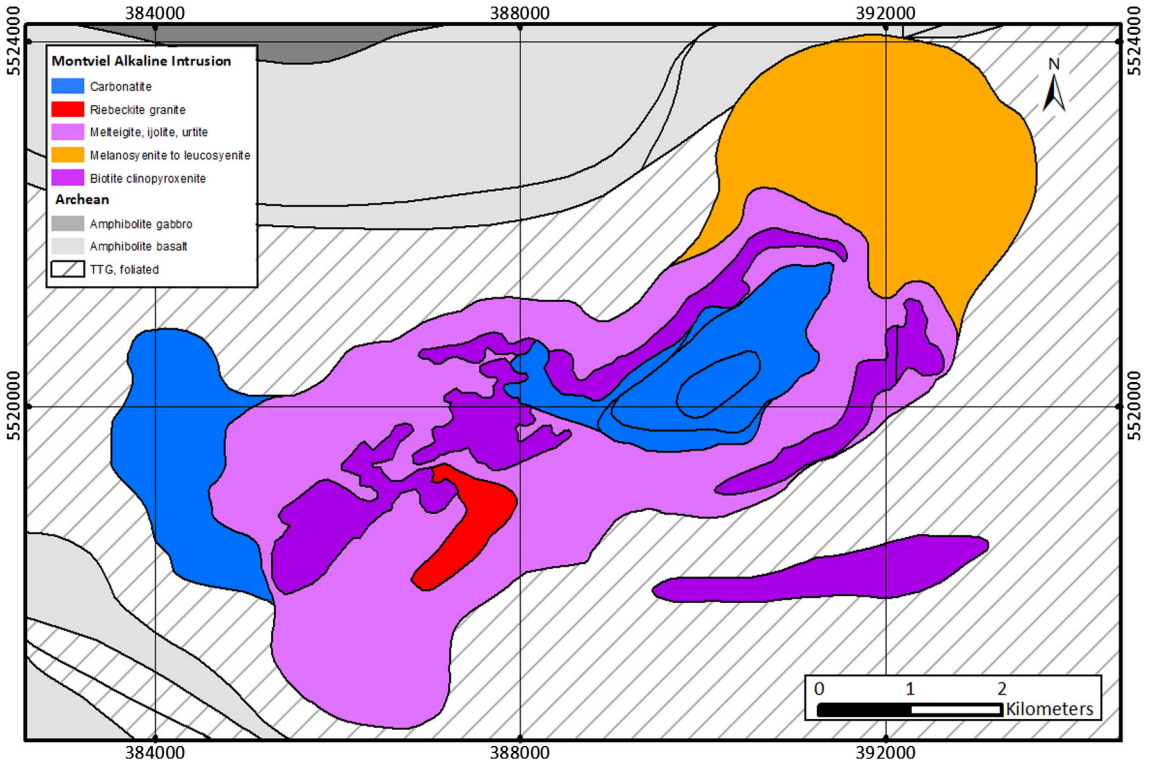

Fig. 2. Geological map of the Montviel intrusion.
Modified after Goutier (2005).

for iron resources in 1958 and exploration continued over 1973–1974 with airborne magnetic surveys and drill core U–Th–Ta assays (Desharnais and Duplessis, 2011). The carbonatite was discovered in 1974 (Barker, 1975) and drilled and assayed for Nb from 1977 to 1979. More drilling and ground electromagnetic surveying was carried on in 2000 in order to verify pre-existing zones of high Nb (Corta and Berthelot, 2002). The property was optioned in 2002 and the potential for P, Nb, REE, Th, fluorite, barite, Cu and PGE was investigated. Airborne magnetic, electromagnetic and radiometric surveys were conducted above the property at 100 m intervals. The first petrographic and mineralogical study, based on microscopic observations and EDX qualitative analyses, reported the existence of Ce–Nd–Ba–Sr–Ca carbonates in the carbonatite (Dumont and Sauvé, 1977; Mulja, 2006). The area was subsequently mapped at the 1:50,000 scale and the intrusion divided in 6 chronological and lithological units, i.e., biotite peridotites and pyroxenites, melano- to leucosyenites, ijolites–urtites–melanosyenites, riebeckite–arfvedsonite granites, Ca and Fe carbonatites and a carbonatite polygenic breccia (Pmtv1 to Pmtv6; Goutier, 2005) (Fig. 2). The intrusion was dated by the U–Pb method on zircon from the ijolite and yielded a crystallization age of 1894 ± 4 Ma (David et al., 2006). Ressources Geomega, who currently own the property, optioned it in 2010 and subsequently conducted 83 diamond drill holes over 4 years totalling 36,500 m. of core, performed a 43-101-compliant resource estimates (an official report required by specific Canadian regulation), mining and engineering pre-economic assessment (PEA), metallurgical tests and environmental studies. The first 43-101 resource estimate of Montviel carbonatites, based on the first 20 drillholes and over 10,000 m of core, reported a total of 183.9 Mt of indicated resources at 1.453 wt.% total rare earth oxides (TREO) and 66.7 Mt of inferred resources at 1.460 wt.% TREO, at a cut-off grade of 1.00 wt.% TREO (Desharnais and Duplessis, 2011). The carbonatite is enriched in Nb and in all rare earth elements, but mostly in Nd, Dy, Eu and Y.

In the present paper, field, drill core, hand sample and conventional optical microscope observations, systematic core sample assays, microscope and scanning electron microscope petrography, electron dispersive X-ray (EDX), X-ray diffraction, electron microprobe (EMP) wavelength dispersive spectrometry (WDS), and laser ablation inductively coupled plasma mass spectrometry (ICP-MS) are integrated to characterize the Montviel carbonatite-hosted REE–Nb deposit. Special emphasis is given to the petrographic relations within the different carbonatite units, the hydrothermal nature of the REE mineralization and to the mineralogy of the REE carbonates and fluorocarbonates. A paragenetic model is proposed on the basis of the above observations, analyses and interpretations.

2. Methodology

Rare earth elements (REE) are typically represented by the 14 lanthanides and by Y, which is also a member of the Group III of the periodic table of the elements. Rare earth elements (REE) are subdivided in terms of light rare earths (LREE; La, Ce, Pr, Nd), medium rare earths (MREE; Sm, Eu, Gd) and heavy rare earths (HREE; Tb, Dy, Y, Ho, Er, Tm, Yb, Lu). Economically critical REEs include Nd (a LREE), Eu (a MREE), Tb, Dy and Y (HREEs), as explained in Section 1.1.

2.1. Drill core assays

Drill cores were analyzed by ALS Val d'Or (Canada) using lithium borate fusion ICP-MS and X-ray fluorescence for Nb. Samples consist of NQ-size half cores normally cut in 1.5 m sections. They were crushed, pulverized, and analyzed for most trace elements. The cores were logged in terms of lithology, texture, mineralization and alteration.

2.2. X-ray diffractometry

Samples of calciocarbonatites, magnesiocarbonatites, ferrocarbonatites, silicocarbonatites and polygenic breccia were crushed, pulverized and scanned using a Siemens D500 X-ray diffractometer equipped with

a Co tube and a Si detector at the Université du Québec à Montréal. X-ray diffraction spectra were identified using Eva software version 1.3.

2.3. Petrography

Polished sections of silicocarbonatite, calciocarbonatite, magnesiocarbonatite, ferrocarbonatite and polygenic breccia were prepared and observed using a Leica DMLP petrographic microscope equipped with a Leica DFC450 digital camera and using a Hitachi TM3000 tabletop scanning electron microscope (SEM) equipped with a Bruker Quantax 70 energy dispersive X-ray spectrometer (EDS).

2.4. Electron microprobe and laser ablation ICP-MS analyses

Rare earth carbonates and fluorocarbonates were analyzed for selected major elements (Ca, Ba, Sr, Na, Fe, Mn, Mg, Na, Si, F, La, Ce, Sm, Pr, Nd, Dy, Y) using a JEOL JXA-8900L electron microprobe (EMP) with a 20 μm diameter, 15 kV and 20 nA beam in the Geochemical Laboratories at McGill University, Montreal, Canada. The instrument was calibrated using a set of commercial and in-house standards (Taylor, MAC-REE). Counting time was 20 s for all elements. Care was taken to remove any spectral interference between elements (Williams, 1996). Relative standard deviations (1σ) were generally less than 1% (e.g., CaO = 20 ± 0.2 wt.%) and limits of detection were around 3000 ppm for REE and lower for other major elements.

Attempts to analyze the same crystals for all REE using a laser ablation ICPMS system were made in the Geotop Laboratories at UQAM, Montreal. The system consists of a Photon-machines Analyte.193 G2 Pulse Excimer laser and a Nu Instrument Attom, high resolution, sector field ICPMS. The system was monitored using a NBS610 glass standard and REE quantified using a USGS MACS3 calcite standard. The concentration of RE elements was calculated by using Sr as the internal standard.

3. Results

3.1. Geology

The alkaline–carbonatite intrusion of Montviel is located in the Archean Craton of the Superior, in the NE of the Sub-Province of Abitibi. The Paleoproterozoic (1.894 Ga; David et al., 2006) rocks were intruded into Archean foliated tonalite. The intrusion is neither deformed nor metamorphosed, whereas the enclosing tonalite reaches the amphibolite facies near the intrusion. The carbonatite is well preserved and is cut by a NNW–SSE fault and by a series of second order NE–SW faults, although all faults appear to have allowed very little displacement (Fig. 3). The following section describes the geology and mineralogy of the carbonatite. The specific REE Ba–Sr–Ca–Na carbonate and fluorocarbonate minerals (Figs. 7–8–9) are identified and distinguished in a subsequent section (Section 3.5).

3.1.1. Silicocarbonatite

Silicocarbonatites (SiC) display three different facies. The first facies is a lamprophyre-like, carbonate-rich SiC which consist of phenocrysts of biotite and phlogopite, and pseudomorphs of olivine altered to antigorite, magnesite and ilmenite, in a matrix of dolomite, ankerite, calcite, pyrite, late hematite and quartz and minor to trace amounts of fluorapatite, titanite, cancrinite, REE carbonates and fluorocarbonates, monazite–(Ce) and xenotime–(Y). Some lamprophyre-like SiC are strongly altered and enriched in REE (particularly HREE), and show pseudomorphs of olivine altered to Fe–Mg carbonates (breunnerite or mesitite), Fe–dolomite, Ti–biotite, fluorapatite, Nb–ilmenite, minor amounts of REE carbonates and fluorocarbonates, monazite–(Ce), xenotime–(Y), antigorite, dickite, and late pyrite and quartz. In contrast, some SiC are better described as glimmerites brecciated by carbonates such as calcite, dolomite, ankerite, strontianite and witherite. This second facies of SiC contains minor to trace amounts of fluorapatite,

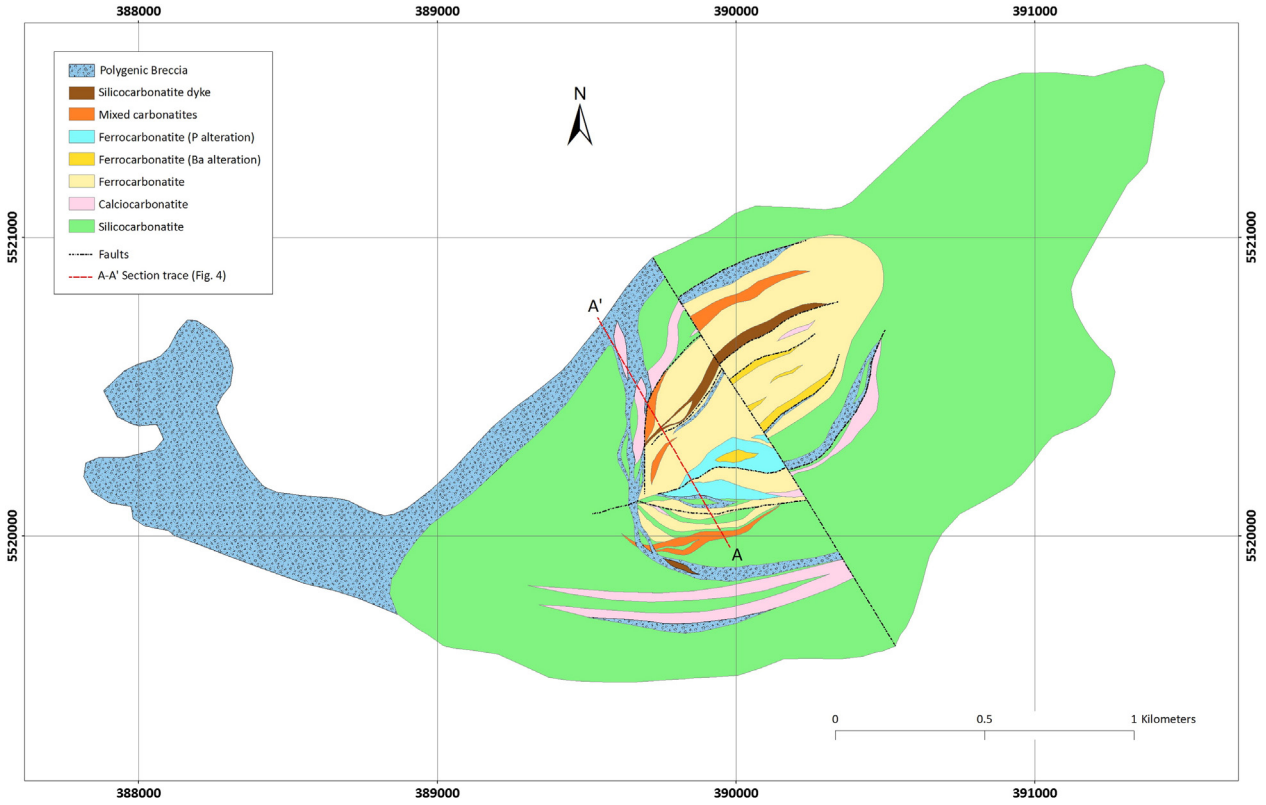

Fig. 3. Geological map of the Montviel carbonatite. Coordinates are in the UTM zone 18 system. The map represents the −50 m level and is thus below the overburden. Ultramafic and alkaline rocks to the north-west of the carbonatite are part of the Montviel intrusion and were mapped by Goutier (2005). Tonalites, trondhjemites and granodiorites (TTG) to the south-east are Archean and host Montviel intrusion (1894 ± 4 Ma, David et al., 2006). All geological mapping was conducted by Ressources Géoméga Inc. under the supervision of A. Cayer.

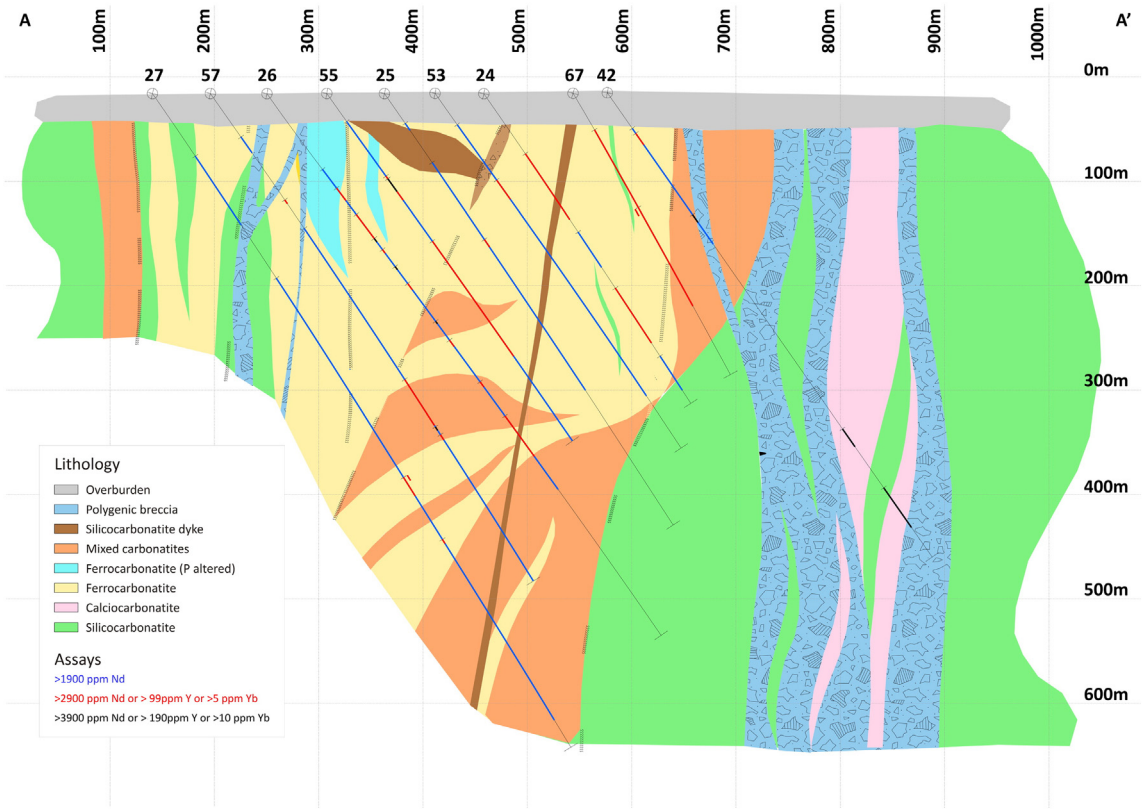

Fig. 4. Geological A–A′ section of the Montviel carbonatite, as seen in Fig. 3. A is to the SSE and A′ is to the NNW. Location of drill holes are drawn and are blue, red and bold black for increasing concentrations of REE. (For interpretation of the references to color in this figure legend, the reader is referred to the web version of this article.)

fluorite, pyrochlore, ilmenite, K feldspar, pyrrhotite, pyrite, chalcopyrite, REE carbonates and fluorocarbonates, monazite–(Ce), xenotime–(Y) and late quartz are also present. In this SiC, the glimmerite hosts Nb in pyrochlore whereas the carbonates host the REE in carbonates and fluorocarbonates. Some apatite in the biotite-rich SiC are metamict and display pleochroic aureoles and some contain numerous melt, fluid, Fe oxide and unidentified Cl-bearing inclusions. Carbonatite melt inclusions are also present in calcite. Based on qualitative EDX analyses coupled to the SEM, F is present in biotite, fluorapatite and fluorite, Ti is present in biotite and ilmenite, Nb is hosted in pyrochlore and ilmenite and Ce is present in apatite. The third facies of SiC is represented by the late SiC dyke crosscutting the carbonatites (Fig. 3), as well as other SiC, which display a brecciated texture and consists of fragments and xenocrysts of Ca–Mg–Fe–Sr–Ba carbonates in a fine matrix of Ti–F–biotite, Fe–dolomite, chlorite, ilmenite, titanite, REE carbonates and fluorocarbonates and pyrite. Mafic to ultramafic enclaves are present and strongly altered. This type of SiC resembles a kimberlite, but with higher amounts of magmatic carbonates, lesser amounts of K-bearing minerals and no fresh olivine.

3.1.2. Magnesiocarbonatite

Magnesiocarbonatites (MgC) are present as rare dykes, pods and lenses that are strongly altered and dominated by dolomite. Ba–Ca–Mg carbonate (Ca-bearing norsethite?), calcite, barytocalcite, strontianite, fluorite, REE carbonates and fluorocarbonates and albite are present in major concentrations. Sphalerite and pyrite occur in minor but significant concentrations. Purple fluorite and zones of Ba alteration within the MgC host globular inclusions with EDX compositions of Ba–Cl–F–Si–O and Ba–Cl–F, equivalent to no existing minerals (except zhangpeishanite, BaFCl; Shimazaki et al., 2008), which in turn host fluorite inclusions. These inclusions are further discussed below.

3.1.3. Calciocarbonatite

Calciocarbonatites (CaC) are dominated by calcite and range from very pure, barren, coarse sövites to LREE-bearing and HREE-bearing hydrothermalized and/or brecciated CaC. Barren sövites consist of coarse calcite with minor to trace amounts of fluorapatite and REE carbonate and fluorocarbonate. Light and heavy REE-bearing CaC also contain major amounts of dolomite, ankerite, strontianite, witherite and barytocalcite and minor to trace concentrations of fluorapatite, barite, REE carbonate and fluorocarbonate, sphalerite, galena and pyrite. Calciocarbonatites contain very few ferromagnesian silicate minerals but do have minor amounts of biotite and aegirine–augite. Chlorite is also present in minor to trace concentrations. The only oxides are late and consist of hematite and goethite.

3.1.4. Ferrocarbonatites

Ferrocarbonatites (FeC) usually cross-cut the CaC, are more strongly hydrothermally altered than the CaC and host more hydrothermal precipitates and most of the REE mineralization, along with the polygenic breccia and the late, mixed carbonatites. They are dominated by ankerite and Fe–dolomite, contain major to minor amounts of siderite, calcite, barytocalcite, strontianite, witherite, fluorite, fluorapatite and secondary hydroxyapatite, as well as minor to trace amounts of biotite, aegirine, arfvedsonite, loparite (a REE-bearing perovskite), barite, REE carbonate and fluorocarbonate, nepheline, sodalite, scapolite, sphalerite and galena. The FeC contain zones that are enriched in LREE or HREE, that display widespread P hydrothermal precipitation dominated by apatite with monazite–(Ce) and xenotime–(Y), and widespread Ba hydrothermal precipitation dominated largely by barytocalcite and Ba–Ca–Mg carbonate, and lesser amounts of witherite, barite and REE carbonate and fluorocarbonate.

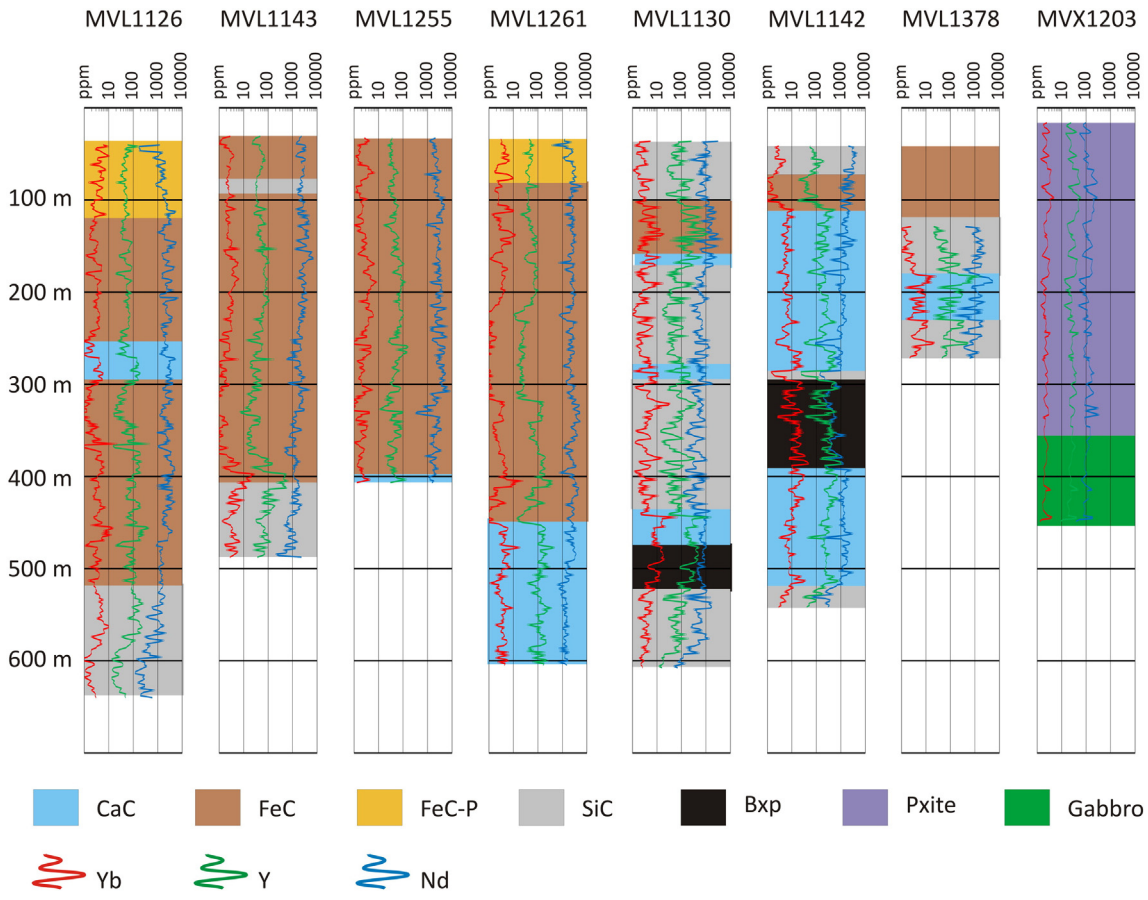

Fig. 5. Core plots showing the concentrations of Nd (a critical LREE), Y and Yb (both critical HREE) in core samples along depth. Depth is in meters and concentration is in ppm on a log scale. Simplified lithology is superimposed for correlation. CaC: calciocarbonatite; FeC: ferrocarbonatite; FeC–P: P_2O_5-altered ferrocarbonatite; SiC: silicocarbonatite; Bxp: polygenic breccia; Pxite: pyroxenite. The first four holes (MVL1126, 1143, 1255 and 1261) display LREE enrichments over a few hundred meters in ferrocarbonatite. The following three holes (MVL1130, 1142 and 1378) show MREE and HREE enrichments in polygenic breccia, ferocarbonatite and calciocarbonatite over intervals of 50 to 100 m. The last hole (MVX1203) represents local, normal values in pyroxenite and gabbro.

3.1.5. Mixed carbonatites

Silicocarbonatites, CaC and FeC similar to those described above appear to have mixed under magmatic conditions (the liquid state) and crosscut pre-existing SiC, CaC and FeC and their hydrothermally altered products with diffused contacts, thus showing up as lenses, dykes and pods. Carbonatites in the magmatic plumbing system thus appear to have been repeatedly injected over prolonged episodes and hydrothermal activity sometimes appears to have preceded mixed SiC–CaC–FeC magmatism. Although REE carbonates and fluorocarbonates are present in significant concentrations in these late mixed carbonatites, they are generally less altered than the pre-existing SiC, CaC and FeC.

3.1.6. Carbonatite polygenic breccia

The polygenic breccia (BXP) is enriched in REE, particularly in HREE, and consists of clasts and xenocrysts of SiC, CaC and FeC in a hydrothermally altered matrix of dolomite, calcite, strontianite, barytocalcite, fluorapatite, biotite, aegirine–augite, and ferro-potassic magnesio-hastingsite. Minor to trace amounts of rutile, magnetite, barite, an Y-Th silicate (huttonite or yttrialite?), a Ce–Ca–Fe–Ti–Nb oxide (aeschynite?), sphalerite, galena, pyrite, REE carbonate and fluorocarbonate were also observed. Nadeau et al. (2013a) determined that the breccia formed as a result of high-energy fragmentation with significant displacement based on modeling of the distribution and size of the fragments in the breccia (Jébrak, 2007). Three dimensional modeling of the deposit based on drill core data (Nadeau et al., 2013a) suggests that the BXP is funnel or diatreme-shaped, which is consistent with the facies of the breccia. The explosion related to the breccia appears to have been the last event of the emplacement of the Montviel intrusion.

3.2. Diamond drill cores

3.2.1. Core plots

The concentration of Nd, Y, and Yb varies with depth in the eight selected drill cores (Fig. 5). In these core plots, the lithologies are superimposed for correlation. However, given that dominant lithologies are systematically cut by dykes, lenses, pods, veins and veinlets of second order lithologies and hydrothermal alterations, only the dominant, first order lithologies were plotted for clarity. The hole number MVX1203 was drilled in barren, relatively fresh pyroxenite and gabbro and represents local normal values, shown here for comparison to the economically enriched Nd (LREE) zones, Y and Yb (HREE) zones. The first four holes (MVL1126, MVL1143, MVL1255 and MVL1261; MVL1126 and MVL1155 are shown as 26 and 55 in Fig. 4) display economically significant LREE enrichments over intervals of a few hundred meters in ferrocarbonatite. Hole MVL1126 shows ranges from about 1000 to 7150 ppm Nd between 110 m and 460 m. Concentration of Nd in hole MVL1143 ranges from about 1000 to 7300 ppm Nd between 110 m and 330 m. Hole MVL1255 displays ranges from about 1000 to 8850 ppm Nd between 85 m and 490 m. By comparison, hole MVX1203 has Nd values ranging around 100 ppm, making the LREE-rich horizons enriched by a factor of 70 to 90 times local normal values.

The following 3 holes (MVL1130, MVL1142 and MVL1378; MVL1142 are shown as 42 in Fig. 4) display HREE enrichments in calciocarbonatite,

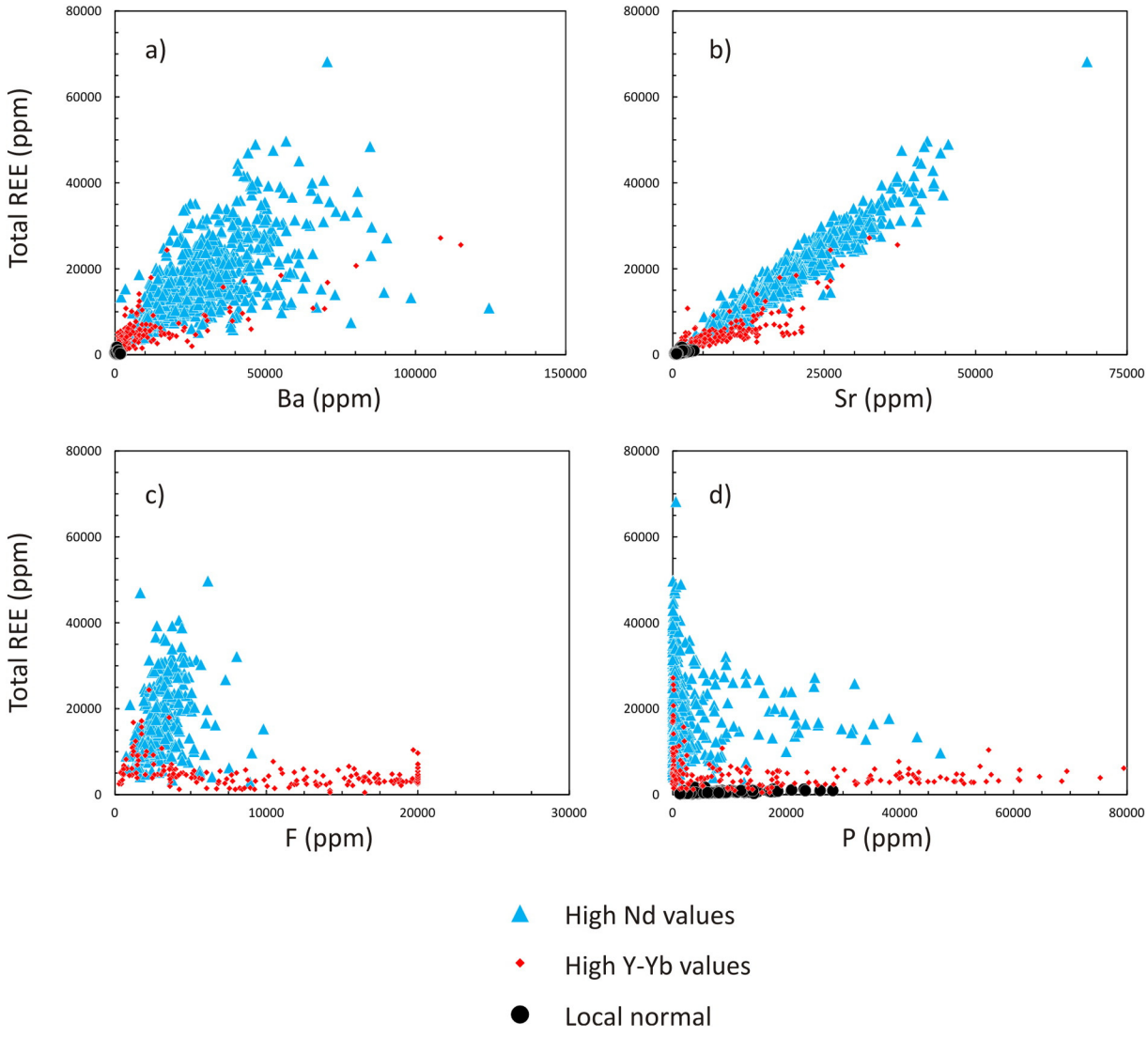

Fig. 6. Lithogeochemical analyses of core samples showing the correlation of total REE content with Sr, Ba, F and P for the Nd-enriched zones, the Y–Yb enriched zones and the local normal values (MVX1203). F was not analyzed in MVX1203.

polygenic breccia and ferrocarbonatite over intervals of 50 to 100 m. Hole MVL1130 shows ranges from about 100 to 1300 ppm Y and 2 to 20 ppm Yb between 110 m and 180 m in ferrocarbonatite. It displays ranges from about 100 to 1660 ppm Y and 1 to 70 ppm Yb between 440 m and 510 m in calciocarbonatite and polygenic breccia. Hole MVL1142 shows ranges from about 10 to 750 ppm Y and 3 to 30 ppm Yb between 230 m and 280 m in calciocarbonatite. It also has ranges from about 3 to 970 ppm Y and 20 to 44 ppm Yb between 300 m and 390 m in polygenic breccia. Hole MVL1378 returned the highest HREE concentrations over its intersection with intermixed calciocarbonatite and ferrocarbonatite (shown as CaC for clarity), between 177 and 195 m, ranging from 28 to 723 Dy, 75 to 1970 ppm Y and 3 to 27 ppm Yb. By contrast, local pyroxenites and gabbros (hole MVX1203) have concentration of around 20 to 40 ppm Y and around 2 ppm Yb, making Y enriched by a factor of 2 to 100 times and Yb enriched by a factor of 2 to 35 times local values.

All of the ore-bearing holes (the first 7 holes) also display a striking 'saw-tooth' pattern, most noticeable when compared to the pyroxenites and gabbros (MVX1203). This saw-tooth pattern varies on the scale of one to a few meters and the high Nd, Y and Yb zones mentioned above are not related to this saw-tooth pattern and correlate better with dominant lithologies. The magmatic relations among pods, lenses and dykes of carbonatites at Montviel are very complex and do vary at this scale. Nevertheless, most carbonatites are hydrothermally altered and this saw-tooth pattern probably originates both because of magmatic and hydrothermal interaction. This is taken up again in the discussion section.

3.2.2. Core assays

The high Nd zones, the high Y and Yb zones and the barren pyroxenites and gabbros described above were used to represent high LREE and high HREE zones and their correlation with Ba, Sr, F and P (Fig. 6). Barium general displays a very good correlation with total REE (TREE) although there is a significant quantity of data scatter (Fig. 6a). The pyroxenite (hole MVX1203; 'local normal' in Fig. 6) has very low Ba and TREE concentrations. Neodymium-rich zones display the greatest amount of scatter in terms of REE and Ba concentration. Most of the Y–Yb-rich zones have relatively low TREE and Ba, and some Y–Yb-rich zones exhibit 2 trends on the diagram, high and low TREE/Ba values. Total REE vs Sr diagram (Fig. 6b) shows excellent correlation although the Nd-zone and the Y–Yb-zone do not plot on the exact same TREE/Sr trend. Local normal pyroxenites and gabbros have low TREE and Sr. Total REE vs F (Fig. 6c) returns different correlations for high Nd values and high Y–Yb values. High LREE ores plot at low (<7000 ppm) F contents and have higher TREE whereas most high HREE ores have high F (greater than 2 wt.%) contents but lower TREE content. F has an upper limit of detection of 20,000 ppm in the bulk assays and could not be

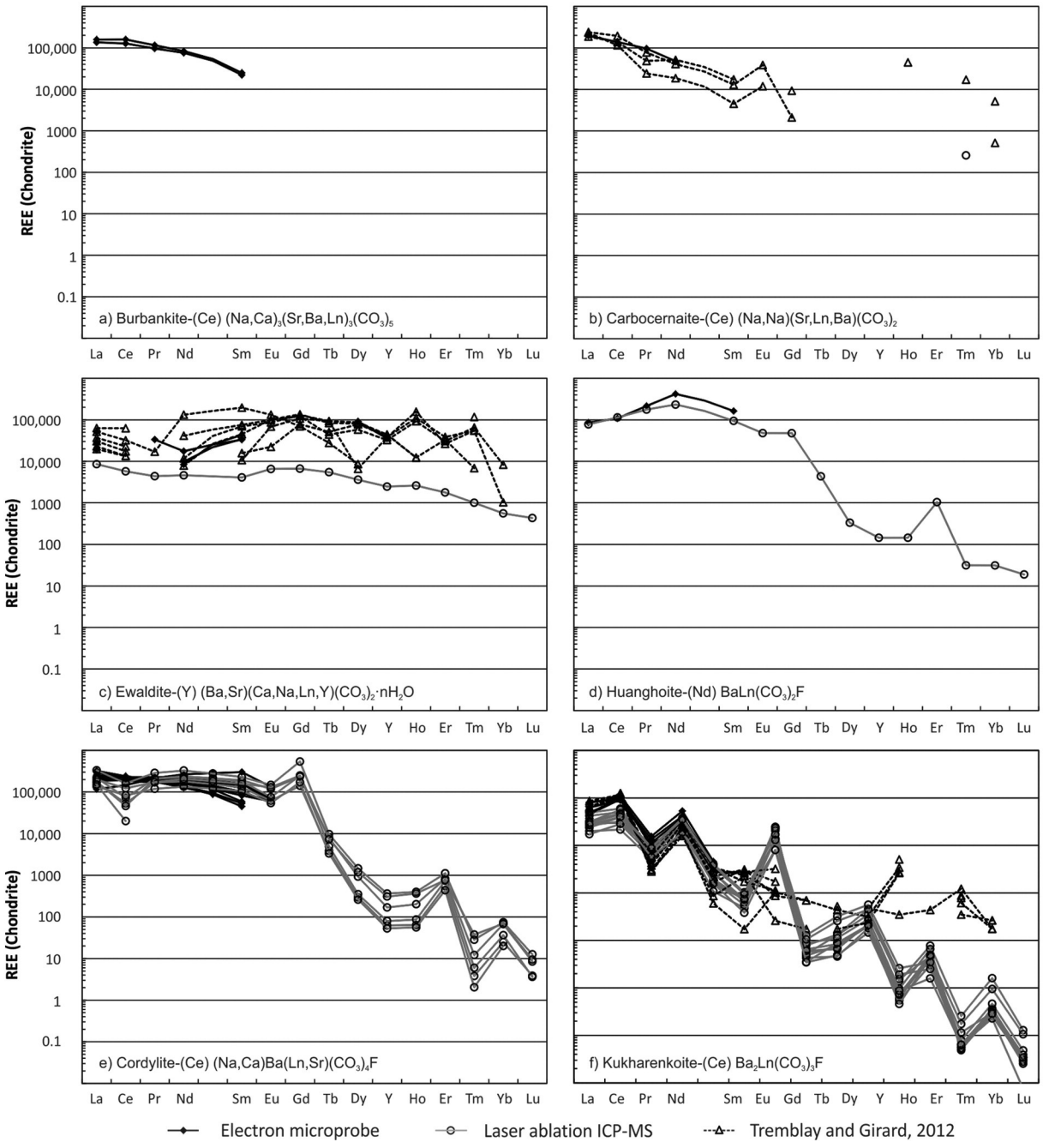

Fig. 7. Rare earth element concentrations in REE-bearing carbonates and fluorocarbonates. 2σ standard deviation error bars on laser ablation ICP-MS was omitted for clarity (see Table 3 for standard deviation values). 1σ relative standard deviations for electron microprobe are also not shown and generally represent 1% of the value. Zhonghuarcerite–(Ce) reported by Tremblay and Girard (2012) is plotted as kukharenkoite–(Ce). Not all of Tremblay and Girard's (2012) zhonghuarcerite–(Ce) data points are plotted for clarity. Notice the different Y-scales for cordylite–(Ce) and kukharenkoite–(Ce) versus other REE carbonates/fluorocarbonates.

plotted for values above this concentration. Fluorine was not analyzed in hole MVX1203. Total REE vs P (Fig. 6d) is similar to TREE vs F as there is no single correlation for both LREE and HREE zones. A significant fraction of the high-Y–Yb zone are abnormally enriched in P (up to 8 wt.%). The highest TREE values are associated with very low P concentrations. Local normal pyroxenites and gabbros have relatively low P concentrations (<3%).

3.3. X-ray diffraction

X-ray diffraction patterns identified the major minerals in silicocarbonatite, LREE-bearing calciocarbonatite, HREE-bearing calciocarbonatite, HREE-bearing, Ba-altered calciocarbonatite, LREE-bearing magnesiocarbonatite, LREE-bearing ferrocarbonatite, F-altered ferrocarbonatite, mixed SiC–CaC–FeC and polygenic breccia (Table 1). X-ray diffraction is sensitive to minerals present in concentrations exceeding 2 to 5 wt.%. Furthermore, X-ray diffraction spectra of calcite, dolomite, ankerite and siderite are very similar, therefore scanning electron microscope observations with EDX analyses are better indicators of carbonate types. The same is true for monazite–(Ce) (LREE phosphate) and xenotime–(Y) (Y and HREE phosphate). Rare earth element-bearing carbonate and fluorocarbonate diffractograms are not reliable as these minerals have variable crystallographic structures and identification databases are not completely populated with existing minerals. Nevertheless, the presence of some of these minerals in XRD analyses confirms their identification

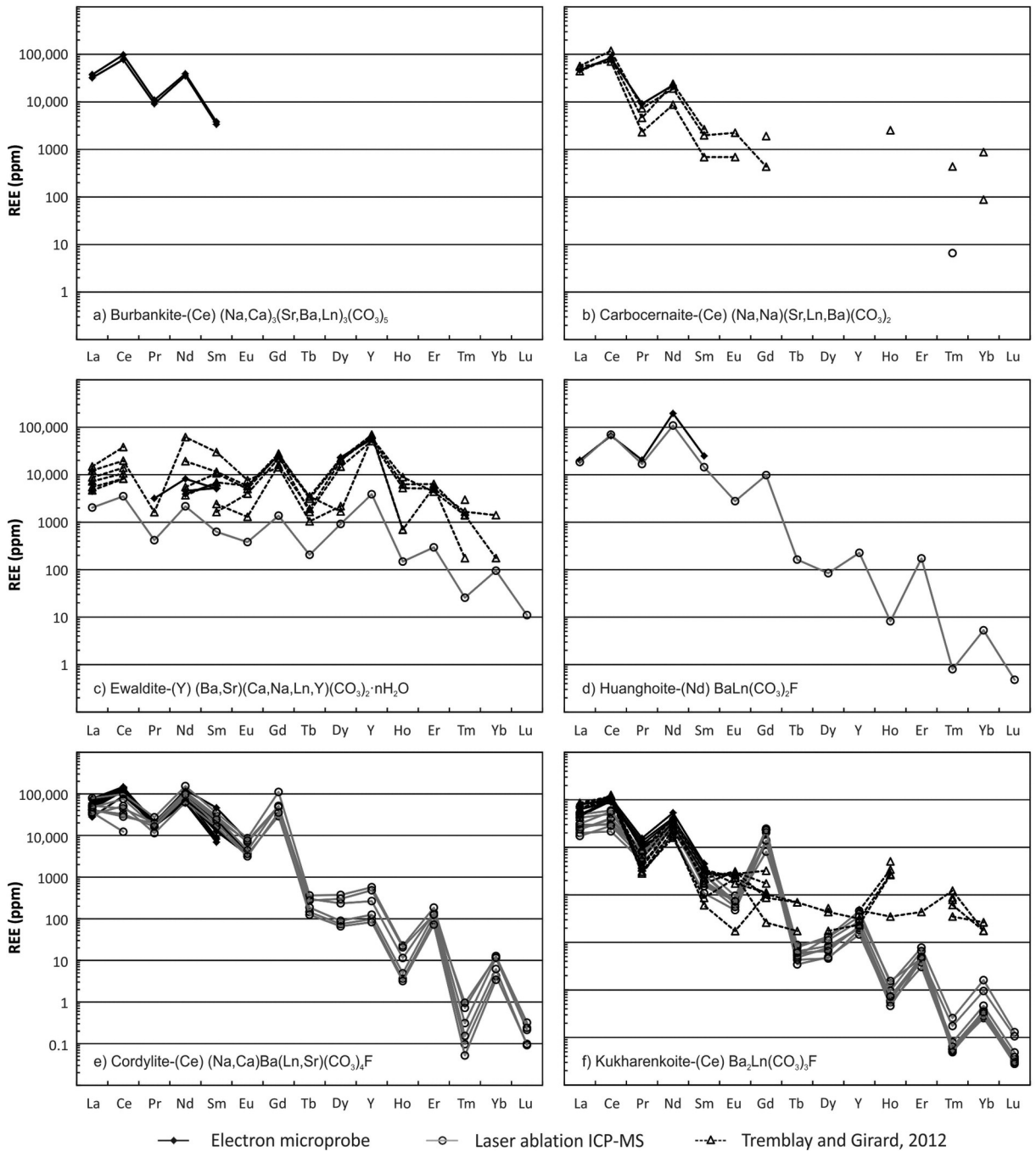

Fig. 8. Chondrite-normalized REE patterns in REE carbonate and fluorocarbonates. 2σ standard deviation error bars on laser ablation ICP-MS were omitted for clarity (see Table 3 for standard deviation values). 1σ relative standard deviations for electron microprobe are also not shown and generally represent 1% of the value. Zhonghuarcerite–(Ce) reported by Tremblay and Girard (2012) is plotted as kukharenkoite–(Ce). Not all of Tremblay and Girard's (2012) zhonghuarcerite–(Ce) data points are plotted for clarity.

using microbeam techniques (see below) and suggests their significant concentrations. For example, burbankite–(Ce) was identified in LREE-bearing calciocarbonatite both by XRD and EMP, huanghoite–(Ce) and kukharenkoite–(Ce) were identified in LREE-bearing ferrocarbonatite both by XRD and EMP (although the huanghoite was a huanghoite–(Nd)), whereas cordylite–(Ce) and cebaite–(Ce) was identified only using the XRD and are thus probably absent.

3.4. Petrography of REE carbonates and fluorocarbonates

Transmitted light photomicrographs of REE-bearing carbonates and fluorocarbonates shown in Fig. 9 are described below. Most of the REE carbonates and fluorocarbonates were altered, occasionally showing magmatic textures and subsequent hydrothermal recrystallization.

A 2 cm phenocryst with burbankite–(Ce)-like composition, i.e., a Na–Ca–Sr–Ba–REE (hydrated?) carbonate is altered to brownish aphanitic phases and hosted in calciocarbonatite (Fig. 9a). Ewaldite–(Y), a Dy–Y–Ba–Sr–Ca–Na hydrated carbonate of the mckelveyite group is fresh, clear and translucent on one hand and brownish and altered on the second hand, within the same photomicrograph of calciocarbonatite (Fig. 9b). In a mixed SiC–CaC–FeC lithology, a centimer-size phenocryst of what probably is qaqarssukite–(Ce), a Ba–Ca–Sr–REE fluorocarbonate (based on EDS spectra), displays a darker altered inner zone within a clearer, fresher outer zone and high order birefringence colors (Fig. 9c). Also within mixed carbonatite lithologies, brownish burbankite–(Ce), a

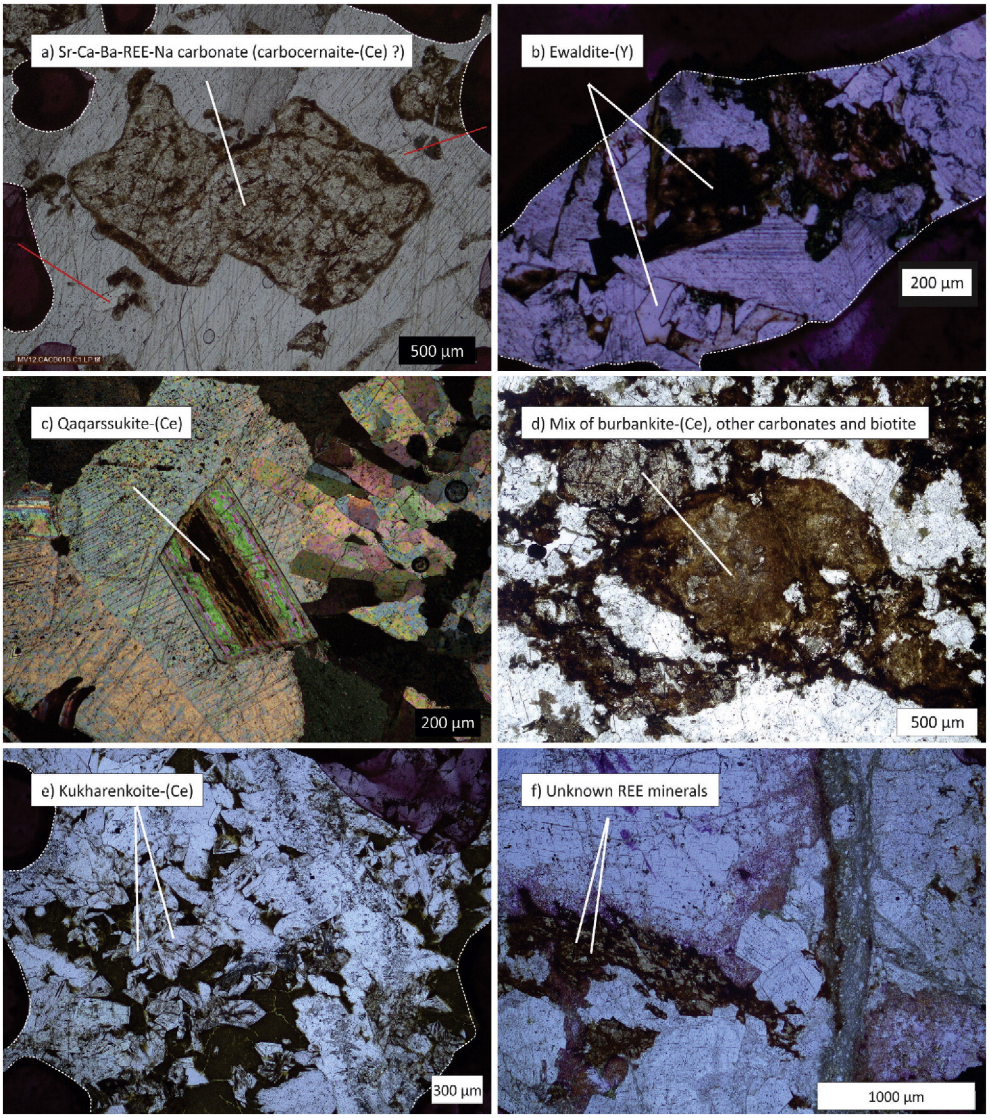

Fig. 9. Photomicrographs of REE-bearing carbonates and fluorocarbonates in carbonatites from Montviel. Photomicrographs are taken in single-polarized light except in 9c. (a) 2 mm phenocryst of undifferentiated Sr–Ca–Ba–REE–Na carbonate in LREE-bearing calciocarbonatite. Although the EDX spectra suggest carbocernaite–(Ce), the mineral is a mixture of fresh and alteration minerals and no pure electron microprobe analyses could be performed (sample MV12.CACB01B). The REE carbonate is surrounded by calcite and apatite is also present (red lines); (b) millimetric HREE-bearing ewaldite–(Y) from an Y–Yb-enriched zone in a calciocarbonatite (sample MV12.HREE02B). Both the translucent (fresh) and the brownish (altered) minerals are HREE-rich ewaldite–(Y), in a matrix of calcite; (c) Crossed polars view of what probably is qaqarssukite–(Ce) in a matrix of calcite–siderite–strontianite–barytocalcite, from a mixed ferrocarbonatite–calciocarbonatite–silicocarbonatite (sample MV12.LATE2); (d) Brownish mixture of REE-bearing minerals, composed mainly of burbankite–(Ce), accompanied by calcite, barytocalcite and biotite in mixed calciocarbonatite–ferrocarbonatite–silicocarbonatite (sample MV13.CACMIX); (e) multiple translucent and fresh crystals of kukharenkoite–(Ce) with dolomite, ankerite, strontianite, chlorite and amphibole in ferrocarbonatite (sample LP12.CAFECB01A); (f) brownish to greenish altered, unknown REE mineral in the presence of purple fluorite, dolomite and strontianite in magnesiocarbonatite (sample LP12.FECB01). Black ink spots are highlighted using white dotted lines to avoid confusion. (For interpretation of the references to color in this figure legend, the reader is referred to the web version of this article.)

Na–Ca–Sr–Ba–REE carbonate, is shown in a mixture with other REE-bearing and non REE-bearing minerals such as barytocalcite, biotite and other aphanitic and unidentifiable minerals (Fig. 9d). Multiple, relatively fresh crystals of what could be kukharenkoite–(Ce), a Ba–REE fluorocarbonate, is intimately associated with brownish alteration zones within ferrocarbonatite (Fig. 9e). Unknown, gray-greenish REE-bearing minerals are associated with purple fluorite, brownish biotite and other ferromagnesian, aphanitic minerals in magnesiocarbonatite (Fig. 9f).

Backscattered electron (BSE) images shown in Fig. 10 are used to illustrate aspects of the REE-bearing hydrothermal alteration. Euhedral, highly altered, lighter fluorapatite from calciocarbonatite is filled with inclusions of darker hydroxyapatite and iron oxides (Fig. 10a; some of the pale-dark contrast is due to charge accumulation, as can be seen in the upper-left corner of the apatite). A BSE close-up view of the altered burbankite–(Ce)-like mineral from calciocarbonatite in Fig. 9a is filled with lighter, REE-bearing patches and stringers, showing that REE were remobilized after their initial crystallization (Fig. 10b). A BSE view of the pervasively altered matrix of the polygenic breccia shows a large crystal of REE-bearing phase, two dark crystals of fluoropotassic amphibole and a groundmass of lighter apatite, darker biotite, and veinlets of barite (Fig. 10c). A zone of high Sr- and F-alteration within the magnesiocarbonatite shows a mixed Ba–Ca–Sr carbonate, fluorite and inclusions of an unidentified Ba–Cl–F–Si–O phase, within a matrix of dolomite (Fig. 10d). A close-up view of one of the inclusions shows that these inclusions in turn host 2–5 µm size mineral inclusions of fluorite (Fig. 10e). Fig. 10f does not pertain to alteration but instead shows an apatite-hosted, calciocarbonatite melt inclusion. The apatite was in a zone of magma mixing between clinopyroxenite and biotite–

Table 1
X-ray diffraction mineral identification. Minerals identified using XRD are given for lithologies in which they were identified.

	SiC	CaC-L	CaC-H	CaC-H (Ba)	MgC-L	FeC-L	FeC-F	Mixed	BXP
Aegirine									✓
Aegirine–augite	✓		✓						✓
Albite					✓				
Ankerite	✓	✓	✓		✓	✓	✓	✓	✓
Antigorite	✓								
Barytocalcite				✓					
Biotite	✓	✓	✓			✓		✓	✓
Burbankite		✓							
Calcite	✓	✓	✓			✓		✓	✓
Calcite, magnesian			✓						
Cancrinite	✓								
Cebaite					✓	✓			✓
Chlorite			✓						
Clinochlore			✓			✓		✓	
Cordylite				✓					
Dickite	✓								
Diopside		✓							
Dolomite	✓	✓	✓		✓	✓			✓
Dolomite, ferroan	✓		✓			✓	✓	✓	✓
Fluorapatite	✓	✓	✓				✓		✓
Fluorite							✓		
Forsterite, ferroan									✓
Glaucophane			✓						
Hedenbergite–jadeite									✓
Hematite	✓								
Hollandite, strontian								✓	
Huanghoite						✓			
Kaolinite			✓						
Kukharenkoite						✓			
Magnetite									✓
Monazite	✓	✓	✓			✓			
Muscovite					✓			✓	
Orthoclase								✓	
Paufferite						✓			
Phlogopite	✓							✓	✓
Qaqarssukite	✓	✓	✓						
Quartz	✓	✓	✓					✓	✓
Siderite						✓		✓	
Sphalerite, ferroan								✓	
Strontianite			✓	✓		✓		✓	✓
Synchysite		✓							
Witherite				✓					
Xenotime	✓	✓	✓	✓		✓	✓	✓	

calciocarbonatite. This melt inclusion was analyzed for major elements using the electron microprobe and for trace elements using laser ablation ICP-MS (Table 4).

These transmitted light photomicrographs and BSE images illustrate the omnipresence of REE, Na, Ba, Sr, F and P in the hydrothermal fluids associated with REE mineralization as well as in the host carbonatite. These fluids could be related to fluids observed in fluid inclusions and potentially also to denser fluids, which we term 'melts' and that seem to have been composed of Ba, F, and Cl (±Si–O) (Fig. 9d–e; discussed further below).

3.5. Rare earth element minerals

3.5.1. Major element concentrations and mineral identification

No pure REE fluorocarbonate (bastnäsite–(Ce)) was identified at the Montviel deposit and the identification of the different REE carbonates and fluorocarbonates was challenging. Burbankite–(Ce) [$(Na,Ca)_3(Sr,Ba,Ln)_3(CO_3)_5$], (Ln is here taken to represent all REE, Y included. Y is specified in addition to Ln for ewaldite–(Y) to emphasize the fact that Y is present as a major element in ewaldite–(Y) carbocernaite–(Ce) [$(Ca,Na)(Sr,Ln,Ba)(CO_3)_2$], ewaldite–(Y) [$(Ba,Sr)(Ca,Na,Ln,Y)(CO_3)_2\cdot nH_2O$], huanghoite–(Nd) [$BaLn(CO_3)_2F$], cordylite–(Ce) [$(Na,Ca)Ba(Ln,Sr)(CO_3)_4F$], kukharenkoite–(Ce) [$Ba_2Ln(CO_3)_3F$], synchysite–(Ce) [$CaLn(CO_3)_2F$], unknown minerals and mixtures of REE carbonate and fluorocarbonate minerals were analyzed and identified based on Ba–Sr–Ca–Na–Ln stoichiometric ratios determined from electron microprobe analyses (Table 2). Although zhonghuacerite–(Ce) has been referred to before in the scientific literature, having the same chemical formula as kukharenkoite–(Ce) (Fleischer et al., 1982), its existence is still a matter of debate and it has not been accepted by the International Mineralogical Association. It was not taken into consideration in the present paper and minerals with this formula were named kukharenkoite–(Ce).

The formulas above agree with those of the Handbook of Mineralogy of the Mineralogical Association of America (MAC), except for a few differences described hereafter. Ewaldite–(Y) is reported by the MAC to have the formula $Ba(Ca,Y,Na,K)(CO_3)_2\cdot nH_2O$ although we have decided to adopt $(Ba,Sr)(Ca,Na,Ln,Y)(CO_3)_2\cdot nH_2O$ because at Montviel Sr often replaces Ba (and Ca) making Sr-rich varieties of the pure minerals.

Minerals did not return exact stoichiometric ratios due to: (1) the presence of solid solutions among end members; (2) alteration and mixtures between minerals; (3) inclusions within the minerals; and (4) because not all REE were analyzed by the electron microprobe. Nevertheless, mineral names could be derived for most analyses.

3.5.2. REE concentrations in ore minerals

A subset of these ore minerals was analyzed for REE using laser ablation ICP-MS (LAICPMS; Figs. 7–8; Table 3). Electron microprobe (EMP) analyses of REE carbonates and fluorocarbonates from both this study and that of Tremblay and Girard (2012) are also reported on the same

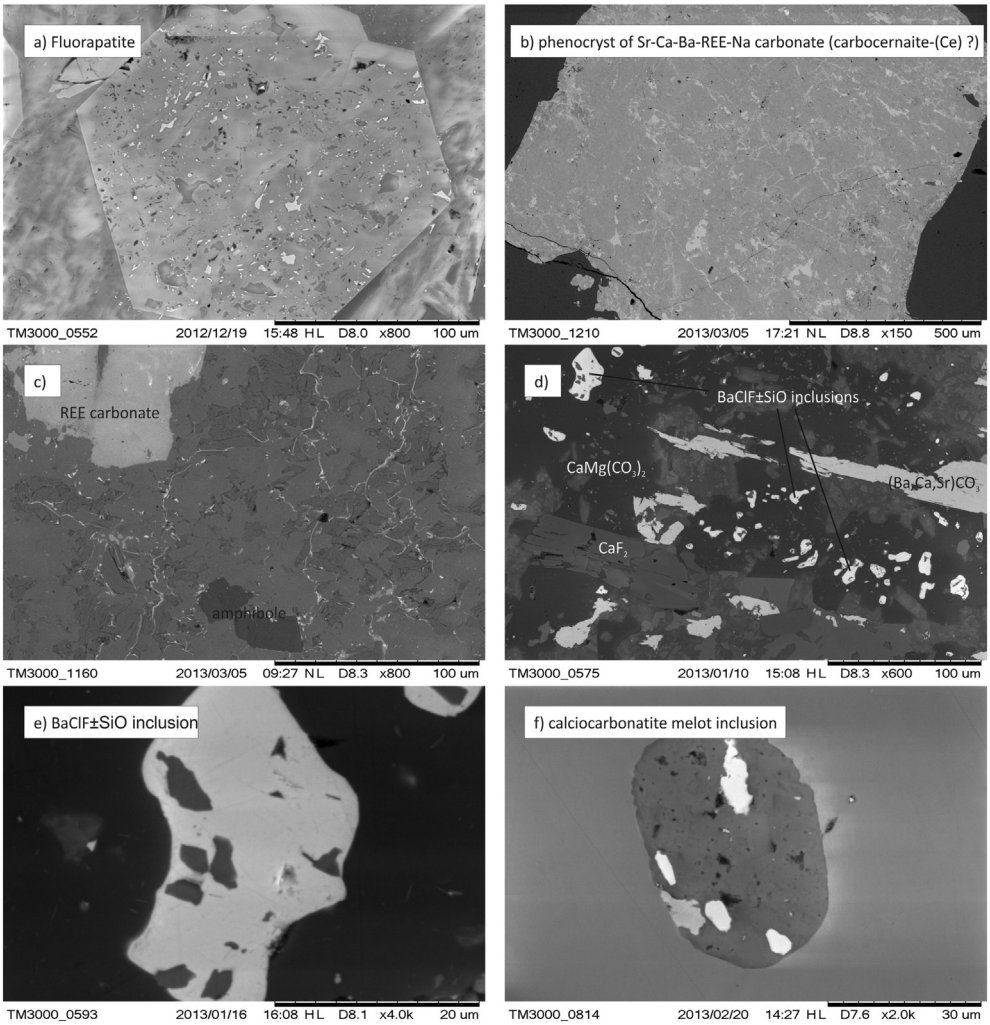

Fig. 10. Backscattered electron (BSE) images showing mineral textures and alteration in carbonatites. (a) Highly metasomatized fluorapatite filled with hydroxyapatite (darker) and Fe oxide inclusions (brighter), from a calciocarbonatite (sample LP12.CACB01A); (b) BSE view of the undifferentiated Sr–Ca–Ba–REE–Na carbonate seen in plain polarized light in Fig. 4a, showing intense alteration into other REE-bearing minerals (sample MV12.CACB01B); (c) BSE view of the matrix of the polygenic breccia. The large, light gray crystal in the upper left corner is a REE-bearing carbonate. The dark crystal in the middle–low part is ferropotassic amphibole. The matrix consists of fluorapatite, a variety of carbonates and biotite and is cut by veinlets of barite and biotite (sample MV12.MBX04.C1); (d) BSE view of an altered area within a magnesiocarbonatite sample. The darker matrix mineral is dolomite and is accompanied by Ba–Ca–Sr carbonates and fluorite. Numerous globular inclusions seem to have caused the alteration and consist of Ba–Cl–F–Si–O (sample LP12.FECB01); (e) close-up view of a Ba–Cl–F–Si–O globules showing inclusions of fluorite crystals (sample LP12.FECB01); (f) apatite-hosted calciocarbonatite melt inclusion with heterogeneously trapped barytocalcite and an unidentified phase. The apatite was in carbonatite in magmatic contact with clinopyroxenite. The composition of the inclusions is reported in Table 4.

diagrams. The concentration of REE in the ore minerals range over 6 orders of magnitude, with Ce reaching up to about 20.2 wt.% in cordylite–(Ce) (Tremblay and Girard, 2012), and Tm and Lu reaching down to about 0.1 ppm in qaqarssukite–(Ce) and in an unidentified mineral.

Significant discrepancy exists between electron microprobe and laser ablation ICP-MS data points, especially for heavy REE concentrations. This discrepancy can be observed for ewaldite–(Y) (Fig. 7c) although the existence of only one LAICPMS data point limits the comparison. This discrepancy is best observed in kukharenkoite–(Ce) (Fig. 7f) for Ho and heavier REE (Ho, Er, Tm, Yb, Lu). This is attributed to interference problems between HREE X-ray signals under the microprobe (Williams, 1996; Tremblay and Girard, 2012) so the LAICPMS data is preferred.

Light REE (LREE; La–Ce–Pr–Nd) are more concentrated than medium REE (MREE) and heavy REE (HREE), and range from about 400 ppm to about 20.2 wt.% in concentration. On average, each LREE was approximately 4.9 ± 4.5 wt.% (1σ standard deviation) and the REE minerals have total LREE around 19.3 wt.%. Neodymium, the only critical LREE, ranges from 2160 ppm to 19.55 wt.% and averages around 4.4 ± 3.3 wt.%.

Medium REE (Sm–Eu–Gd) have concentrations that are intermediate between LREE and HREE, ranging from about 173 ppm to about 11.1 wt.%. and averaging individually around 0.7 wt.%. Europium, the only critical MREE, ranges between 173 ppm and 0.86 wt.% and averages around 0.3 wt.%. Minerals have an average total of 2.2 wt.% MREE.

Heavy REE (Tb–Dy–Y–Ho–Er–Tm–Yb–Lu) are most depleted, ranging from 0.1 ppm to about 7.0 wt.% and averaging around 2220 ppm. Significant differences exist between the concentrations of the different HREE and we put the emphasis on the critical HREE, i.e., Tb, Dy and Y. Terbium ranges from 35 ppm to 0.35 wt.% and averages around 500 ppm. Dysprosium is significantly enriched, ranging from 46 ppm to about 2.3 wt.%, averaging around 0.3 wt.%. Yttrium is also significantly enriched, ranging from 79 ppm to about 0.70 wt.% and averaging around 1.0 wt.%. The heavier HREE's average concentrations decrease with Z (the nb. of protons) so Ho, Er, Tm, Yb and Lu have average concentrations of 1265, 689, 344, 148 and 3 ppm, respectively.

Although REE concentrations are highly variable, almost all minerals have similar REE concentration patterns, showing up to tens of wt.% LREE and gradually less medium and heavy REEs. Ewaldite–(Y) is a significant exception and displays MREE and HREE enrichments relative to

other minerals, with Eu ranging from 381 ppm to 0.77 wt.% (average 4286 ppm), Tb ranging from 205 to 3475 ppm (average 2127 ppm), Dy ranging from 918 to 2.3 wt.% (average 1.5 wt.%) and Y ranging from 3880 ppm to 7.0 wt.% (average 5.4 wt.%). The concentration of heavier HREE in ewaldite–(Y) remains uncertain since the electron probe data is inaccurate and only one laser ablation ICP-MS data point was obtained. Gadolinium, a MREE, stands out slightly positively of the REE concentration patterns determined from LAICPMS in huanghoite–(Nd) and ewaldite–(Y), and stands out even more strongly in qaqarssukite–(Ce) and kukharenkoite–(Ce). Given the discrepancy between Gd concentrations obtained from the EMPA and that obtained from the LAICPMS in kukharenkoite–(Ce), it is possible that this might have resulted from analytical error. Neodymium also appears to be anomalously enriched in huanghoite–(Nd) and cordylite–(Ce) and cordylite–(Nd) although for Nd this is observed via both EMPA and LAICPMS methods.

Rare earth concentrations were normalized to chondrites (Sun and McDonough, 1989) to get a sense of the light-to-heavy REE factors and to verify the presence of specific element anomalies (Fig. 8). Most minerals display very strong negative REE patterns with Lu generally around 10 times chondrite and LREE 10^5 to 10^6 times chondrites.

Burbankite–(Ce), carbocernaite–(Ce) and kukharenkoite–(Ce) have negative and relatively gradual slopes for the LREE. Cordylite–(Ce) has a flat LREE to MREE patterns and displays a relative enrichment in Nd and MREEs (one is actually cordylite–(Nd)). Huanghoite–(Nd) has a positive LREE to MREE slope and displays significant enrichment in Nd and Sm. Ewaldite–(Y) has lower LREE enrichments but strong MREE and HREE enrichments, displaying flat to slightly negative REE patterns. Gadolinium often shows a positive anomaly although this could be due to an analytical error of the LAICPMS.

4. Discussion

4.1. A hydrothermal origin

All rare earth element-bearing carbonates and fluorocarbonates at Montviel host Ba (except 2 EMPA points on mixed minerals in sample LP12.CACB01A.C3; Tables 2–3), usually host Sr and F, and REE phosphates (monazite–(Ce) and xenotime–(Y)) are present in trace to minor amounts almost throughout carbonatite magmatism and hydrothermalism (Fig. 11). From the above and in conjunction with the zones of Ba, Sr, F and P hydrothermal precipitation discussed above, are in agreement with a hydrothermal origin for the REE-bearing phases. The REE carbonates and fluorocarbonates are usually altered, are often present in veinlets or are associated with pockets of hydrothermal minerals (Fig. 9d, e and f). Nevertheless, there are other occurrences where a hydrothermal origin is uncertain and where the minerals could be magmatic (Fig. 9a–c). In these cases, the minerals have been altered and the REE were remobilized. Scanning electron microscope BSE images clearly demonstrate that most minerals were pervasively altered (Fig. 10a–c).

Although fluid inclusions were commonly observed in calcite and apatite, globular inclusions with Ba–Cl–F–Si–O and Ba–Cl–F compositions and hosted in dolomite were observed in close association with mineralization and alteration (Fig. 10d–e). These suggest the existence of immiscible barium chloro-fluoro-silicate and/or barium chlorofluoride 'melts' at the origin of some of the alteration. Although to our knowledge no such 'melt' has ever been reported, the textures displayed by these inclusions suggest a molten state, they are intimately associated to zones of Ba, Sr and F hydrothermal phases, and minerals with Ba–Cl–F–Si–O have never been reported. Since no mineral exist with this composition, the possibility that these globules resulted from partial dissolution of pre-existing minerals is excluded. Furthermore, no other mineral around these globules host Si so it could not have originated from contamination from surrounding minerals. Mineral inclusions with Ba–Cl–F compositions (without Si–O), named zangpeishanite, were reported in fluorite from the Bayan Obo carbonatite-hosted REE deposit (Shimazaki et al., 2008) and it is interesting to note that the minerals present within the inclusions at Montviel are fluorite and thus appear to have been heterogeneously trapped (Fig. 10d–e), as if fluorite was crystallizing from a Ba–Cl–F–Si–O melt. It is possible that BaFCl (±Si–O) melts could be at the origin of some of the Ba and F alteration. The rocks contain very little chlorine although evidence of a hydrothermal fluid was preserved as fluid inclusions and minerals with chlorine such as sodalite and scapolite were identified by the scanning electron microscope EDX system. Although the ephemeral nature, and sometimes the water solubility, of immiscible melts have made them difficult to identify and thus remain highly controversial, it has been demonstrated that they can transport significant concentrations of REE (Klemme, 2004; Veksler, 2005; Veksler et al., 2005, 2012; Vasykuova and Williams-Jones, 2013; Vasyukova and Williams-Jones, 2014). We suggest that a Ba–Cl–F (±Si–O) melt has contributed to the hydrothermal precipitation, REE transport and mineralization at Montviel, although we recognize that more work is required in order to fully understand the nature of these Ba–Cl–F (±Si–O) melts. At Montviel mineral crystallization from BaClF (±Si–O) melts remains undistinguishable from that originating from hydrothermal fluids. Hence, we broadly refer to alteration with no implication on the physico-chemical nature of the fluid, whether it is the H_2O–CO_2-based fluid or the BaFCl (±Si–O)-based fluid which caused the alteration and mineralization.

The signatures of REE mineral precipitation, alteration and remobilization are seen as 'saw tooth' patterns in the drill core plots (Fig. 5). Hydrothermal fluids seem to have remobilized the REE at the meter scale, thus creating alternating zones of relatively REE-rich and REE-poor regions within host lithologies. However, the LREE-rich zones of holes MVL1126, MVL1143, MVL1255 and MVL1261 and the HREE-rich zones of holes MVL1130, MVL1142 and MVL1378 do not seem to be related to this short scale remobilization because the zones are larger and do not oscillate at the meter scale (Figs. 4–5). These mineralization zones are thus more akin to principal host lithologies and the ore fluids thus appear to have been injected simultaneously with the magmas. This suggests that the ore fluid did not circulate after magma emplacement but that the mineralizing process stemmed from the intrusion of volatile-saturated carbonatite magma with concurrent autometasomatism by magmatic fluids.

4.2. REE minerals and concentrations

Absolute REE concentrations in REE carbonates and fluorocarbonates vary over 6 orders of magnitude, from ppm-level HREE to 20 wt.% LREE. Chondrite-normalized patterns for these carbonates and fluorocarbonates show extreme LREE enrichments of 10^5 to 10^6 times chondrite and relatively low HREE enrichments of about 10 times chondrite, returning LREE/HREE ratios around 10^4. In contrast, the calciocarbonatite melt inclusion (Fig. 10f; Table 4) has a total REE content of 186 ppm, a LREE enrichment of about 100–150 times chondrite and a HREE enrichment of about 2 times chondrite.

Since all REE minerals are either altered or of unequivocal hydrothermal origin, partitioning can be measured between a mineralizing fluid and REE minerals, although according to Samson and Wood (2005), in silica-bearing systems, REE generally prefer to remain in the melt over the fluid. Fluid/melt K_d increase with the chlorinity of the fluid and is greater for LREE than HREE resulting in orthomagmatic, Cl-rich aqueous fluids enriched in LREE compared to the silicate melt. In the silicate melt–carbonatite melt–CO_2 system, in the absence of H_2O, at 1200 °C to 1300 °C and 0.5 to 2 GPa, $K_{Ce}^{CO_2\ vapor/carbonate\ melt} \approx 5$ to $20, K_{Sm}^{CO_2\ vapor/carbonate\ melt} \approx 0.5$ to 3 and $K_{Tm}^{CO_2\ vapor/carbonate\ melt} \approx 0.3$ *to* 3.5 (Wendlandt and Harrison, 1979), showing that carbonic hydrothermal fluids can be greatly enriched in REE compared to magmas and significantly enriched in LREE compared to HREE. This is consistent with more recent experimental work documenting the mobility of REE and

Table 2
Rare earth element-bearing, carbonate and fluorocarbonate mineral major element concentrations, structural formulae and mineral name determination. Oxides are in wt.%. Silicium was analyzed to monitor contamination. Ln stands for any REE, Y included. CO_2 was calculated so microprobe total was 100%.

Mineral	Ideal formula	Structural formula	BaO	SrO	CaO	Na_2O	F	MgO	FeO	La_2O_3	Ce_2O_3	Pr_2O_3	Nd_2O_3	Sm_2O_3	Eu_2O_3	Dy_2O_3	Y_2O_3	SiO_2	CO_2	Total	Sample
Burbankite–(Ce)	$(Na,Ca)3(Sr,Ln,Ba)3(CO_3)_5$	$(Na,Ca)_{3.64}(Sr,Ln,Ba)_{2.54}C_{4.95}O_{14.91}F_{0.09}$	11.0	23.6	6.9	12.9	0.25		0.2	3.1	6.5	0.8	2.2						32.2	100.0	MV12.MBX04.C1.P1
Burbankite–(Ce)	$(Na,Ca)3(Sr,Ln,Ba)3(CO_3)_5$	$(Na,Ca)_{3.53}(Sr,Ln,Ba)3.0_4C_{4.76}O_{14.94}F_{0.06}$	2.4	29.0	2.5	14.1	0.17		0.2	4.4	11.4	1.3	4.5	0.4					29.6	100.0	MV13.CACMIX.C1.P1
Burbankite–(Ce)	$(Na,Ca)3(Sr,Ln,Ba)3(CO_3)_5$	$(Na,Ca)_{3.64}(Sr,Ln,Ba)_{2.54}C_{4.95}O_{14.91}F_{0.09}$	5.6	18.1	3.9	13.6	0.43	0.1	7.8	5.2	10.3	1.2	3.5					0.5	29.5	100.0	MV13.CACMIX.C2.P2
Burbankite–(Ce)	$(Na,Ca)3(Sr,Ln,Ba)3(CO_3)_5$	$(Na,Ca)_{3.40}(Sr,Ln,Ba)_{2.88}C_{4.83}O_{15.00}F_{0.00}$	2.9	29.3	2.9	13.5			2.0	3.8	9.1	1.1	4.1	0.4					30.5	100.0	MV13.CACMIX.C2.P3A
Burbankite–(Ce)	$(Na,Ca)3(Sr,Ln,Ba)3(CO_3)_5$	$(Na,Ca)_{3.50}(Sr,Ln,Ba)_{2.79}C_{4.67}O15.00F_{0.00}$	4.3	25.6	2.6	13.8			5.4	4.0	9.6	1.2	3.8	0.3					28.8	100.0	MV13.CACMIX.C2.P3B
Carbocernaite–(Ce)	$(Ca,Na)(Sr,Ln,Ba)(CO_3)_2$	$(Ca,Na)_{0.83}(Sr,Ln,Ba)_{0.83}C_{2.14}O_{5.96}F_{0.05}$	4.1	20.3	12.6	3.6	0.37		1.3	5.5	9.9	1.1	2.6						38.5	100.0	MV13.FECL1.C2.P1
Carbocernaite–(Ce)	$(Ca,Na)(Sr,Ln,Ba)(CO_3)_2$	$(Ca,Na)_{1.08}(Sr,Ln,Ba)_{1.02}C_{1.93}O_{5.95}F_{0.05}$	5.8	21.9	14.1	4.5	0.38		0.7	5.8	10.9	1.1	3.3						31.3	100.0	MV13.FECL1.C2.P2
Ewaldite–(Y)	$(Ba,Sr)(Ca,Na,Ln,Y)(CO_3)_2 \cdot nH_2O$	$(Ba,Sr)_{0.84}(Ca,Na,Ln,Y)_{0.90}C_{2.16}O_{6.00}F_{0.00}\neg nH_2O$	36.7	6.7	5.0	4.3				1.4			0.5	0.8		2.7	7.5		34.2	100.0	MV12.HREE02B.C2.P1
Ewaldite–(Y)	$(Ba,Sr)(Ca,Na,Ln,Y)(CO_3)_2 \cdot nH_2O$	$(Ba,Sr)_{0.83}(Ca,Na,Ln,Y)_{0.80}C_{2.21}O_{6.00}F_{0.00}\neg nH_2O$	38.7	5.4	4.4	4.0				0.7			0.6	0.9	0.5	1.9	6.8		35.7	100.0	MV12.HREE02B.C2.P3
Ewaldite–(Y)	$(Ba,Sr)(Ca,Na,Ln,Y)(CO_3)_2 \cdot nH_2O$	$(Ba,Sr)_{0.78}(Ca,Na,Ln,Y)_{0.85}C_{2.18}O_{6.00}F_{0.00}\neg nH_2O$	33.3	7.7	4.9	4.4			1.9	0.8			0.5	0.6		2.7	7.1		35.7	100.0	MV12.HREE02B.C3.P1
Ewaldite–(Y)	$(Ba,Sr)(Ca,Na,Ln,Y)(CO_3)_2 \cdot nH_2O$	$(Ba,Sr)_{0.83}(Ca,Na,Ln,Y)_{0.80}C_{2.21}O_{6.00}F_{0.00}\neg nH_2O$	38.0	4.7	4.5	4.4				0.5		0.4	1.0	0.6		2.6	7.7		35.3	100.0	MV12.HREE02B.C3.P2
Huanghoite–(Nd)	$BaLn(CO_3)_2F$	$Ba_{0.73}Ln_{0.80}C_{1.74}O_{5.32}F_{0.68}$	32.0	2.7	1.0		3.70		1.5	2.4	7.8	2.4	22.8	2.9				0.2	22.0	100.0	MV13.FECBAL.C1.P1
Cordylite–(Ce)	$(Na,Ca)Ba(Ln,Sr)(CO_3)_4F$	$(Na,Ca)_{1.19}Ba_{1.03}(Ln,Sr)_{1.63}C_{4.12}O_{11.86}F_{1.14}$	23.9	3.7	4.0	3.4	3.28		0.1	6.2	13.6	1.9	10.2	2.8	0.5				27.5	100.0	MV12.CAFECB02.C3.P1
Cordylite–(Ce)	$(Na,Ca)Ba(Ln,Sr)(CO_3)_4F$	$(Na,Ca)_{1.04}Ba_{0.95}(Ln,Sr)_{1.54}C_{4.05}O_{11.91}F_{1.09}$	22.6	4.3	3.7	2.9	3.22	0.4	2.1	7.7	15.4	2.0	6.8	0.8				1.1	27.7	100.0	MV12.HREE02.C1.P1BIS
Cordylite–(Ce)	$(Na,Ca)Ba(Ln,Sr)(CO_3)_4F$	$(Na,Ca)_{0.89}Ba_{1.04}(Ln,Sr)_{1.80}C_{4.00}O_{12.04}F0_{.96}$	23.4	4.2	5.1	1.2	2.67		1.0	8.0	17.2	2.4	8.2	1.1			0.2	0.3	25.9	100.0	MV12.HREE02B.C1.P1
Cordylite–(Ce)	$(Na,Ca)Ba(Ln,Sr)(CO_3)_4F$	$(Na,Ca)_{1.09}Ba_{0.95}(Ln,Sr)_{1.62}C_{4.24}O_{11.99}F_{1.01}$	22.6	3.4	2.3	4.0	2.99		0.4	6.8	16.2	2.4	9.6	1.0				0.2	29.0	100.0	MV12.HREE05.C1.P2
Cordylite–(Ce)	$(Na,Ca)Ba(Ln,Sr)(CO_3)_4F$	$(Na,Ca)_{1.19}Ba_{1.11}(Ln,Sr)_{1.70}C_{4.06}O_{12.03}F_{0.97}$	25.1	4.7	4.4	3.1	2.73			5.4	13.8	2.2	10.5	2.3				0.2	26.4	100.0	MV12.LATE2.C1.P1A
Cordylite–(Nd)	$(Na,Ca)Ba(Ln,Sr)(CO_3)_4F$	$(Na,Ca)_{1.16}Ba_{0.99}(Ln,Sr)_{1.71}C_{4.07}O_{11.97}F_{1.03}$	22.9	3.8	4.4	3.0	2.95		0.2	3.2	10.5	2.4	14.5	5.4	0.9			0.2	26.9	100.0	MV12.LATE2.C1.P1B
Cordylite–(Ce)	$(Na,Ca)Ba(Ln,Sr)(CO_3)_4F$	$(Na,Ca)_{0.75}Ba_{0.92}(Ln,Sr)_{1.60}C_{4.11}O_{12.15}F_{0.85}$	21.7	3.7	4.6	1.0	2.50	0.1	2.7	5.7	13.8	2.1	10.8	2.6				1.2	27.8	100.0	MV12.LATE2.C2.P1A
Cordylite–(Ce)	$(Na,Ca)Ba(Ln,Sr)(CO_3)_4F$	$(Na,Ca)_{0.57}Ba_{0.56}(Ln,Sr)_{1.93}C_{4.47}O_{12.44}F_{0.56}$	13.9	7.2	3.5	0.9	1.72		0.8	6.2	16.2	2.5	12.5	2.8	0.4				32.0	100.0	MV12.LATE2.C2.P1B
Cordylite–(Ce)	$(Na,Ca)Ba(Ln,Sr)(CO_3)_4F$	$(Na,Ca)_{1.14}Ba_{1.15}(Ln,Sr)_{1.77}C_{4.00}O_{11.94}F_{1.06}$	25.7	4.7	4.1	2.9	2.93			5.2	13.9	2.4	11.2	2.2	0.5				25.6	100.0	MV12.LATE2.C2.P1C
Cordylite–(Ce)	$(Na,Ca)Ba(Ln,Sr)(CO_3)_4F$	$(Na,Ca)_{0.92}Ba_{0.96}(Ln,Sr)_{1.62}C_{4.14}O_{12.00}F_{1.00}$	22.6	3.8	4.1	2.1	2.92		1.3	7.9	14.9	2.3	8.2	1.6				0.7	27.9	100.0	MV12.LATE3.C1.P1
Cordylite–(Ce)	$(Na,Ca)Ba(Ln,Sr)(CO_3)_4F$	$(Na,Ca)_{0.96}Ba_{0.90}(Ln,Sr)_{1.63}C_{4.28}O_{12.15}F_{0.85}$	21.5	3.6	3.8	2.5	2.52		0.4	7.2	15.1	2.5	9.7	1.8				0.2	29.4	100.0	MV12.LATE3.C1.P1B

(continued on next page)

Table 2 (*continued*)

Mineral	Ideal formula	Structural formula	BaO	SrO	CaO	Na_2O	F	MgO	FeO	La_2O_3	Ce_2O_3	Pr_2O_3	Nd_2O_3	Sm_2O_3	Eu_2O_3	Dy_2O_3	Y_2O_3	SiO_2	CO_2	Total	Sample
Cordylite–(Ce)	$(Na,Ca)Ba(Ln,Sr)(CO_3)_4F$	$(Na,Ca)_{1.02}Ba_{0.92}(Ln,Sr)_{1.64}C_{4.23}O_{12.07}F_{0.93}$	21.9	4.6	4.4	2.5	2.76		0.6	7.1	15.2	2.2	8.9	1.5				0.1	29.0	100.0	MV12.LATE3.C1.P1C
Cordylite–(Ce)	$(Na,Ca)Ba(Ln,Sr)(CO_3)_4F$	$(Na,Ca)_{1.05}Ba_{1.03}(Ln,Sr)_{1.61}C_{4.22}O_{11.98}F_{1.02}$	24.4	4.1	3.2	3.2	3.00		0.2	8.4	15.9	2.1	7.1	0.8					28.6	100.0	MV12.LATE3.C2.P1A
Cordylite–(Ce)	$(Na,Ca)Ba(Ln,Sr)(CO_3)_4F$	$(Na,Ca)_{1.09}Ba_{1.06}(Ln,Sr)_{1.77}C_{4.05}O_{11.98}F_{1.02}$	24.1	4.0	3.5	3.1	2.86		0.2	9.0	17.2	2.1	7.4	0.9				0.2	26.3	100.0	MV12.LATE3.C2.P1B
Cordylite–(Ce)	$(Na,Ca)Ba(Ln,Sr)(CO_3)_4F$	$(Na,Ca)_{0.94}Ba_{0.98}(Ln,Sr)_{1.68}C_{4.22}O_{12.03}F_{0.97}$	23.1	4.4	3.9	2.3	2.84		0.3	8.9	16.8	2.0	7.0	1.0					28.5	100.0	MV12.LATE3.C2.P1C
Cordylite–(Ce)	$(Na,Ca)Ba(Ln,Sr)(CO_3)_4F$	$(Na,Ca)_{1.01}Ba_{0.94}(Ln,Sr)_{1.66}C_{4.17}O_{12.01}F_{0.99}$	22.2	4.0	3.4	2.9	2.90		1.0	7.1	16.0	2.0	8.7	1.7	0.4			0.3	28.2	100.0	MV12.LATE3.C4.P1A
Cordylite–(Ce)	$(Na,Ca)Ba(Ln,Sr)(CO_3)_4F$	$(Na,Ca)_{1.11}Ba_{1.06}(Ln,Sr)_{1.73}C_{4.105}O_{11.83}F_{1.17}$	24.2	3.9	3.8	3.0	3.32			8.2	15.9	2.0	8.7	1.5	0.4				26.5	100.0	MV12.LATE3.C4.P1B
Synchysite–(Ce)	$CaLn(CO_3)_2F$	$Ca_{0.89}Ln_{0.75}C_{2.13}O_{6.06}F_{0.94}$	1.5	0.9	17.0		6.12	0.5	1.2	9.9	20.8	2.4	8.3	0.6			0.2	1.1	32.0	100.0	MV12.UMBX01.C3.P2
Kukharenkoite–(Ce)	Ba_2LnCO_3F LP12.CAFECB01A.C1.P1	$Ba_{1.77}Ln_{0.89}C_{3.08}O_{8.74}F_{1.26}$	47.1	1.4	0.1	0.1	4.13			9.5	11.6	1.2	2.9						23.5	100.0	
Kukharenkoite–(Ce)	Ba_2LnCO_3F LP12.CAFECB01A.C2.P1	$Ba_{1.93}Ln_{0.90}C_{3.02}O_{8.78}F_{1.22}$	49.2	1.3		0.1	3.88			9.3	11.6	1.2	2.5						22.1	100.0	
Kukharenkoite–(Ce)	Ba_2LnCO_3F LP12.CAFECB01A.C3.P2	$Ba_{1.86}Ln_{0.87}C_{3.08}O_{8.77}F_{1.23}$	48.6	0.8		0.1	3.97	0.1		7.6	11.8	1.5	3.6						23.1	100.0	
Kukharenkoite–(Ce)	Ba_2LnCO_3F	$Ba_{2.05}Ln_{0.92}C_{2.94}O_{8.75}F_{1.25}$	51.0	0.7	0.2	0.2	3.86			9.5	11.3	1.2	2.4						21.0	100.0	LP12.UMBX01.C4.P1
Kukharenkoite–(Ce)	Ba_2LnCO_3F	$Ba_{2.00}Ln_{0.90}C_{2.95}O_{8.65}F_{1.35}$	50.7	0.4	0.3	0.1	4.23			9.0	11.5	1.2	2.6						21.4	100.0	LP12.UMBX01.C5.P1
Kukharenkoite–(Ce)	Ba_2LnCO_3F	$Ba_{1.73}Ln_{1.02}C_{2.82}O_{8.64}F_{1.36}$	44.3	1.2	0.4	0.1	4.33	0.3	1.4	7.6	14.1	1.7	4.6				0.7		20.8	100.0	MV12.UMBX01.C3.P1
Kukharenkoite–(Ce)	$Ba_3Ln(CO_3)xF_2$	$Ba_{2.01}Ln_{0.85}C_{2.98}O_{8.83}F_{1.17}$	50.8	0.7	0.5	0.3	3.65	0.1	0.4	5.3	11.0	1.6	4.8	0.4					21.6	100.0	MV13.CACMIX.C1.P2
Kukharenkoite–(Ce)	$Ba_3Ln(CO_3)_xF_2$	$Ba_{2.02}Ln_{0.84}C_{3.02}O_{8.75}F_{1.25}$	51.7	0.5	0.1	0.2	3.95			5.8	10.9	1.3	4.5	0.5					22.1	100.0	MV13.CACMIX.C2.P1
Kukharenkoite–(Ce)	Ba_2LnCO_3F	$Ba_{1.82}Ln_{0.96}C_{2.95}O_{8.88}F_{1.12}$	46.7	1.5	0.8	0.1	3.56			5.1	12.9	1.8	6.2	0.5			0.4	21.7	100.0	MV13.FECL2.C1.P1
Kukharenkoite–(Ce)	Ba_2LnCO_3F	$Ba_{1.74}Ln_{0.77}C_{2.57}O_{8.95}F_{1.05}$	46.3	0.8	0.2	0.4	3.47	2.6	1.7	7.4	10.4	1.3	2.8				4.3	19.6	100.0	LP12.UMBX01.C1.P1
Kukharenkoite–(Ce)	Ba_2LnCO_3F LP12.CAFECB01A.C3.P1	$Ba_{1.62}Ln_{0.75}C_{3.30}O_{8.83}F_{1.17}$	46.2	1.2		0.1	4.14			7.9	10.6	1.4	2.9						26.9	100.0	
Kukharenkoite–(Ce)	Ba_2LnCO_3F LP12.CAFECB01A.C5.P1	$Ba_{1.86}Ln_{0.79}C_{3.15}O_{8.83}F_{1.17}$	49.4	1.2		0.1	3.87			7.5	10.7	1.4	3.0						24.0	100.0	
Kukharenkoite–(Ce)	Ba_2LnCO_3F	$Ba_{1.92}Ln_{0.84}C_{3.08}O_{8.72}F_{1.28}$	50.0	0.8	0.1	0.1	4.11			8.9	10.7	1.2	2.8						22.8	100.0	LP12.FECB01B.C3.P1
Kukharenkoite–(Ce)	Ba_2LnCO_3F	$Ba_{1.84}Ln_{0.74}C_{3.10}O_{8.79}F_{1.21}$	49.3	1.1	0.4	0.1	3.99		1.4	5.8	10.1	1.2	3.8	0.5					23.8	100.0	MV12.HREE02B.C2.P2
Kukharenkoite–(Ce)	Ba_2LnCO_3F	$Ba_{1.90}Ln_{0.78}C_{3.11}O_{8.81}F_{1.19}$	50.1	1.0	0.4	0.1	3.88			5.1	10.3	1.3	4.8	0.6					23.5	100.0	MV12.HREE03.C1.P1
Kukharenkoite–(Ce)	Ba_2LnCO_3F	$Ba_{1.76}Ln_{0.75}C_{3.18}O_{8.82}F_{1.18}$	48.0	1.1	0.8	0.2	4.00			6.1	11.0	1.3	3.6						25.0	100.0	MV12.HREE03.C1.P2
Kukharenkoite–(Ce)	Ba_2LnCO_3F	$Ba_{1.94}Ln_{0.83}C_{3.07}O_{8.81}F_{1.19}$.	50.3	0.8	0.2	0.1	3.83			6.4	11.4	1.3	3.9						22.9	100.0	MV12.HREE03.C2.P1A
Kukharenkoite–(Ce)	Ba_2LnCO_3F	$Ba_{1.95}Ln_{0.82}C_{3.08}O_{8.80}F_{1.20}$	50.5	0.8	0.1	0.1	3.87			6.3	11.2	1.3	3.9						23.0	100.0	MV12.HREE03.C2.P1B
Kukharenkoite–(Ce)	Ba_2LnCO_3F	$Ba_{1.95}Ln_{0.80}C_{3.08}O_{8.76}F_{1.24}$	50.6	0.8	0.1	0.1	3.98			6.6	10.7	1.5	3.6						23.0	100.0	MV12.HREE03.C2.P1C
Kukharenkoite–(Ce)	Ba_2LnCO_3F	$Ba_{1.92}Ln_{0.83}C_{3.07}O_{8.78}F_{1.22}$	49.9	0.7	0.1	0.1	3.93		0.3	6.3	10.9	1.6	4.1	0.4					23.0	100.0	MV12.HREE03.C3.P1
Kukharenkoite–(Ce)	Ba_2LnCO_3F	$Ba_{1.83}Ln_{0.75}C_{3.14}O_{8.84}F_{1.16}$	49.4	0.7	0.2	0.2	3.86		0.8	5.1	9.5	1.6	5.1	0.4				0.3	24.3	100.0	MV12.HREE05.C1.P1
Unknown mineral		14.5	1.0		0.43	0.9	2.1	10.5	26.3	3.2	10.1	0.8						1.9	28.2	100.0	MV12.SICACB02.C3.P1
Unknown mineral	21.6	3.2	2.5	3.5	2.76	2.4	2.1	10.6	18.4	1.7	4.8							4.9	22.4	100.0	MV13.DYK1.C1.P1
Unknown mineral	19.9	4.2	5.8	0.2	4.14	7.1	3.9	6.8	12.5	1.4	5.3	0.6						7.7	21.9	100.0	MV13.DYK2.C1.P1
Mixture	0.4	0.6	18.2		5.99		6.1	9.3	19.8	2.3	7.5	0.6					0.1	0.2	31.1	100.0	LP12.CACB01A.C3.P1
Mixture	0.4	0.6	17.6	0.1	5.73	0.1	8.7	8.2	17.8	2.2	6.8	0.5					0.2	0.3	33.1	100.0	LP12.CACB01A.C3.P2
Mixture	0.5	0.5	18.6		6.36	0.1	4.8	9.4	18.2	2.4	7.5	0.7					0.1	0.5	32.7	100.0	LP12.CACB01A.C4.P1
Mixture	9.1	25.0	16.6	2.5				4.8	5.2	0.5	0.9								35.2	100.0	MV12.CACB01B.C2.P1 mixture
Mixture	8.7	27.0	16.9	2.2				3.3	4.4	0.4	0.9								35.9	100.0	MV12.CACB01B.C2.P2 mixture
Mixture	4.5	29.3	17.8	2.1				2.1	4.8	0.9	2.0								36.0	100.0	MV12.CACB01B.C2.P3 mixture
Mixture	4.9	24.4	7.6	12.2			2.7	2.7	6.1	0.6	3.0	0.6							34.9	100.0	MV12.MBX03.C1.P1
Mixture	4.7	24.3	7.6	12.8	0.73	0.1	1.3	3.8	7.3	0.9	2.9								33.9	100.0	MV12.MBX03.C1.P2
Mixture	34.8 MV12.UMBX01.C1.P1Amix	1.4	4.4	0.1	4.64		1.1	8.0	16.0	1.7	5.3							1.9	22.3	100.0	
Mixture	2.7 MV12.UMBX01.C1.P1Bmix	1.0	17.6		5.92		0.7	9.1	19.8	2.2	8.0	0.5					0.2	4.8	29.9	100.0	

Table 3
Rare earth element-bearing carbonate and fluorocarbonate REE element concentrations as obtained from laser ablation ICPMS. All results are in ppm.

Mineral	Lithology	La	Ce	Pr	Nd	Sm	Eu	Gd	Tb	Dy	Y	Ho	Er	Tm	Yb	Lu
		Concentration (ppm)														
Carbocernaite–(Ce)	Ferrocarbonatite, LREE													7		
Ewaldite–(Y)	Calciocarbonatite, MREE	2030	3520	418	2160	627	381	1370	205	918	3880	148	295	26	95	11
Huanghoite–(Ce)	Ferrocarbonatite, LREE, Ba–alteration	18,480	69,800	16,790	108,700	14,400	2780	9800	163	84	227	8	173	1	5	0.5
Kukharenkoite–(Ce)	Carbonatitic biotite breccia	42,100	50,300	8240	27,100	1771	718	23,800	56	70	211	6	47	1	4	0.3
Kukharenkoite–(Ce)	Carbonatitic biotite breccia	24,000	39,200	6510	27,300	2690	633	8100	79	133	459	14	78	3	16	1
Kukharenkoite–(Ce)	Carbonatitic biotite breccia	20,000	21,600	5170	17,030	1081	478	13,400	35	49	146	5	30	1	3	0.3
Kukharenkoite–(Ce)	Carbonatitic biotite breccia	29,800	29,600	7830	26,100	1518	747	22,900	43	46	182	5	43	1	3	0.3
Kukharenkoite–(Ce)	Ferrocarbonatite, dolomitic, LREE	49,100	59,600	7590	23,180	1760	557	23,400	52	129	351	15	46	2	10	1
Kukharenkoite–(Ce)	Ferrocarbonatite, dolomitic, LREE	26,600	31,800	7510	26,400	1940	743	24,600	48	77	200	7	38	1	5	0.5
Kukharenkoite–(Ce)	Mixed CaC–FeC, late	23,800	40,800	8330	36,460	3470	959	20,600	88	112	281	10	66	1	4	0.3
Kukharenkoite–(Ce)	Mixed CaC–FeC, late	17,300	28,300	6030	26,040	2595	730	14,000	65	84	204	7	46	1	3	0.3
Kukharenkoite–(Ce)	Mixed CaC–FeC, late	31,300	56,300	8170	31,800	2700	728	22,900	61	66	223	7	50	0.5	3	0.4
Kukharenkoite–(Ce)	Polygenic breccia, MREE	32,300	47,100	9260	37,600	4050	1028	17,000	129	321	564	26	35	1	3	0.3
Kukharenkoite–(Ce)	Polygenic breccia, MREE	30,000	45,000	8680	35,300	3860	933	13,000	105	256	449	19	25	1	2	0.1
Kukharenkoite–(Ce)	Polygenic breccia, MREE	27,700	39,800	5700	18,880	1594	383	8000	35	89	211	9	16	1	3	0.3
Cordylite–(Ce)	Mixed CaC–FeC, late	52,300	44,400	20,100	111,600	29,400	6900	48,000	299	235	265	11	137	0.3	11	0.2
Cordylite–(Ce)	Mixed CaC–FeC, late	40,500	32,600	16,200	84,300	19,700	3590	29,100	145	75	98	4	91	0.1	4	0.10
Cordylite–(Ce)	Mixed CaC–FeC, late	41,800	28,400	19,700	108,000	27,600	4380	51,000	186	89	125	5	123	0.2	6	0.09
Cordylite–(Ce)	Mixed CaC–FeC, late	79,100	99,000	27,400	153,600	35,000	8610	111,000	364	373	572	23	185	1	13	0.3
Cordylite–(Ce)	Mixed CaC–FeC, late	47,400	75,400	16,500	96,600	24,200	7560	51,100	275	301	484	21	127	1	12	0.2
Cordylite–(Ce)	Mixed CaC–FeC, late	32,500	50,800	11,370	62,900	16,300	3160	35,400	125	66	83	3	72	0.1	3	1200
Cordylite–(Ce)	Mixed CaC–FeC, late	35,800	12,300													
Mixture	Calciocarbonatite, LREE	22,700	31,500	7730	33,400	3160	706	4670	92	226	625	27	80	4	26	2
Mixture	Calciocarbonatite, LREE	25,000	34,400	7530	35,100	3510	731	4270	108	250	716	29	89	4	25	3
Mixture	Calciocarbonatite, LREE	31,100	46,600	7850	33,200	3290	915	3270	95	238	607	26	75	4	25	2
Mixture	Calciocarbonatite, LREE	16,300	24,600	4350	18,300	1820	461	2260	55	135	364	17	48	3	18	2

Table 3 (*continued*)

Mineral	Lithology	La	Ce	Pr	Nd	Sm	Eu	Gd	Tb	Dy	Y	Ho	Er	Tm	Yb	Lu
		2σ standard deviations														
Carbocernaite–(Ce)	Ferrocarbonatite, LREE												17,000	5		
Ewaldite–(Y)	Calciocarbonatite, MREE	140	220	36	210	85	46	330	22	95	290	17	38	5	18	3
Huanghoite–(Ce)	Ferrocarbonatite, LREE, Ba–alteration	470	2300	420	3300	590	120	1500	8	8	16	1	9	0.2	1	0.2
Kukharenkoite–(Ce)	Carbonatitic biotite breccia	3700	4900	220	1000	84	64	4200	3	4	7	1	2	0.1	1	0.1
Kukharenkoite–(Ce)	Carbonatitic biotite breccia	2000	3700	330	1100	150	55	1600	4	9	24	1	6	0.3	2	0.2
Kukharenkoite–(Ce)	Carbonatitic biotite breccia	2500	3100	160	790	55	51	1700	2	4	8	0.4	2	0.1	0.3	0.05
Kukharenkoite–(Ce)	Carbonatitic biotite breccia	3500	4300	200	1100	59	69	3400	2	2	5	0.3	2	0.1	0.4	0.1
Kukharenkoite–(Ce)	Ferrocarbonatite, dolomitic, LREE	3300	5100	220	900	81	49	4300	3	9	15	1	4	0.3	1	0.2
Kukharenkoite–(Ce)	Ferrocarbonatite, dolomitic, LREE	3000	4600	210	1400	110	81	3500	3	5	9	0.5	2	0.1	1	0.1
Kukharenkoite–(Ce)	Mixed CaC–FeC, late	1900	4700	240	870	130	62	3200	3	5	9	0.5	3	0.1	0.5	0.1
Kukharenkoite–(Ce)	Mixed CaC–FeC, late	1500	3300	220	650	85	41	2100	2	4	6	0.3	2	0.1	0.4	0.1
Kukharenkoite–(Ce)	Mixed CaC–FeC, late	1900	3900	240	1300	130	54	3700	3	5	11	1	3	0.1	1	0.1
Kukharenkoite–(Ce)	Polygenic breccia, MREE	3100	5000	300	1500	160	36	2000	6	16	50	1	2	0.2	1	0.1
Kukharenkoite–(Ce)	Polygenic breccia, MREE	2800	4800	240	1200	120	26	1800	4	11	15	1	2	0.1	1	0.03
Kukharenkoite–(Ce)	Polygenic breccia, MREE	1700	2900	210	800	69	18	1100	2	6	8	1	2	0.2	1	0.1
Cordylite–(Ce)	Mixed CaC–FeC, late	1300	8600	1300	7100	2400	530	13,000	22	18	19	1	12	0.1	2	0.1
Cordylite–(Ce)	Mixed CaC–FeC, late	1100	6500	1300	7300	1900	380	8000	13	8	8	1	9	0.0	1	0.1
Cordylite–(Ce)	Mixed CaC–FeC, late	2500	5900	2900	17,000	5200	830	18,000	36	16	21	1	22	0.1	1	0.1
Cordylite–(Ce)	Mixed CaC–FeC, late	2800	12,000	1900	8900	1900	660	15,000	30	36	47	3	15	0.3	3	0.2
Cordylite–(Ce)	Mixed CaC–FeC, late	2000	4900	1000	6700	1900	550	9900	20	27	42	2	12	0.3	2	0.1
Cordylite–(Ce)	Mixed CaC–FeC, late	2600	820	4500	1200	290	6800	11	6	5	0.5	8	0.04	1	0.5	0.6
Cordylite–(Ce)	Mixed CaC–FeC, late	3500	3300													
Mixture	Calciocarbonatite, LREE	2300	3700	390	1800	200	33	420	6	14	64	2	5	0.4	2	0.3
Mixture	Calciocarbonatite, LREE	3000	4400	520	2100	210	28	350	8	18	96	2	6	0.4	2	0.3
Mixture	Calciocarbonatite, LREE	2600	4000	450	2100	230	43	290	7	17	60	2	6	0.5	3	0.4
Mixture	Calciocarbonatite, LREE	1400	1900	250	1400	170	40	310	5	13	47	2	5	0.4	2	0.3

Table 3 (*continued*)
Rare earth element-bearing carbonate and fluorocarbonate REE element concentrations as obtained from laser ablation ICPMS. All results are in ppm.

Mineral	Lithology	La	Ce	Pr	Nd	Sm	Eu	Gd	Tb	Dy	Y	Ho	Er	Tm	Yb	Lu	Sample
		Limits of detections															
Carbocernaite–(Ce)	Ferrocarbonatite, LREE	3.9	2.5	1.1	5.6	4.4	4.1	54	1.1	0.1	1.5	0.5	1.5	0.1	3	0.7	MV13.FECL1.C2.P1
Ewaldite–(Y)	Calciocarbonatite, MREE	13.6	10.4	4.0	24.1	0.1	18.5	232	4.6	14.5	8.8	2	7.8	1.8	7.5	2.0	MV12.HREE02B.C2.P1
Huanghoite–(Ce)	Ferrocarbonatite, LREE, Ba–alteration	1.0	0.8	0.3	1.0	1.2	1.5	14	0.3	0.9	0.5	0.1	0.5	0.1	0.7	0.3	MV13.FECBAL.C1.P1
Kukharenkoite–(Ce)	Carbonatitic biotite breccia	0.2	0.1	0.0	0.2	0.1	0.5	3	0.1	0.2	0.1	0.1	0.1	0.03	0.1	0.04	LP12.UMBX01.C1.P1
Kukharenkoite–(Ce)	Carbonatitic biotite breccia	0.1	0.1	0.0	0.0	0.4	0.2	2	0.1	0.1	0.1	0.04	0.1	0.03	0.2	0.04	LP12.UMBX01.C1.P1
Kukharenkoite–(Ce)	Carbonatitic biotite breccia	0.1	0.1	0.0	0.1	0.1	0.2	1	0.03	0.1	0.04	0.02	0.1	0.03	0.1	0.04	LP12.UMBX01.C4.P1
Kukharenkoite–(Ce)	Carbonatitic biotite breccia	0.1	0.2	0.1	0.2	0.1	0.3	2	0.1	0.2	0.1	0.03	0.1	0.04	0.1	0.06	LP12.UMBX01.C4.P1
Kukharenkoite–(Ce)	Ferrocarbonatite, dolomitic, LREE	0.3	0.2	0.1	0.5	0.1	0.7	6	0.2	0.3	0.3	0.06	0.2	0.08	0.3	0.1	LP12.CAFECB01A.C1.P1
Kukharenkoite–(Ce)	Ferrocarbonatite, dolomitic, LREE	0.1	0.1	0.0	0.2	0.1	0.3	3	0.1	0.1	0.1	0.03	0.1	0.04	0.2	0.05	LP12.CAFECB01A.C2.P1
Kukharenkoite–(Ce)	Mixed CaC–FeC, late	0.1	0.1	0.0	0.2	0.1	0.3	2	0.1	0.2	0.1	0.02	0.1	0.03	0.1	0.04	MV13.CACMIX.C1.P2
Kukharenkoite–(Ce)	Mixed CaC–FeC, late	0.2	0.1	0.0	0.2	0.1	0.1	1	0.04	0.1	0.03	0.02	0.1	0.02	0.1	0.03	MV13.CACMIX.C1.P2
Kukharenkoite–(Ce)	Mixed CaC–FeC, late	0.3	0.2	0.1	0.4	0.1	0.4	4	0.1	0.3	0.1	0.09	0.2	0.04	0.2	0.09	MV13.CACMIX.C2.P1
Kukharenkoite–(Ce)	Polygenic breccia, MREE	0.6	0.1	0.0	0.3	0.1	0.1	1	0.1	0.1	0.1	0.1	0.1	0.05	0.1	0.03	MV12.HREE03.C2.P1A
Kukharenkoite–(Ce)	Polygenic breccia, MREE	0.6	0.1	0.0	0.3	0.1	0.1	1	0.1	0.1	0.1	0.1	0.1	0.05	0.1	0.03	MV12.HREE03.C2.P1A
Kukharenkoite–(Ce)	Polygenic breccia, MREE	0.2	0.1	0.0	0.5	0.3	0.3	2	0.1	0.2	0.1	0.1	0.1	0.05	0.2	0.04	MV12.HREE03.C2.P1A
Cordylite–(Ce)	Mixed CaC–FeC, late	0.3	0.2	0.1	0.9	0.1	0.7	4	0.2	0.3	0.1	0.1	0.3	0.05	0.1	0.10	MV12.LATE2.C1.P1A
Cordylite–(Ce)	Mixed CaC–FeC, late	0.2	0.3	0.1	0.3	0.3	0.4	4	0.1	0.3	0.1	0.1	0.2	0.06	0.2	0.09	MV12.LATE2.C1.P1A
Cordylite–(Ce)	Mixed CaC–FeC, late	0.4	0.3	2.2	0.7	0.1	0.4	3	0.1	0.2	0.1	0.1	0.1	0.04	0.1	0.09	MV12.LATE2.C1.P1A
Cordylite–(Ce)	Mixed CaC–FeC, late	1.2	1.1	1.3	2.6	1.7	1.4	15	0.4	0.8	0.4	0.1	0.6	0.03	1.1	0.3	MV12.LATE2.C2.P1A
Cordylite–(Ce)	Mixed CaC–FeC, late	0.7	0.8	0.2	1.1	0.9	0.9	10	0.2	0.6	0.4	0.1	0.5	0.10	0.7	0.2	MV12.LATE2.C2.P1A
Cordylite–(Ce)	Mixed CaC–FeC, late	0.2	3.3	0.7	0.8	6	0.2	0.3	0.1	0.2	0.3	0.08	0.6	0.2	MV12.LATE2.C2.P1C		
Cordylite–(Ce)	Mixed CaC–FeC, late	0.5	0.4	0.1	1.0	0.6	0.5	5	0.1	0.3	0.3	0.16	0.3	0.09	0.1	0.1	MV12.LATE3.C1.P1C
Mixture	Calciocarbonatite, LREE	0.2	0.1	0.1	0.4	0.1	0.3	3	0.05	0.1	0.2	0.03	0.1	0.02	0.1	0.05	LP12.CACB01A.C3.P1
Mixture	Calciocarbonatite, LREE	0.1	0.1	0.0	0.2	0.2	0.3	3	0.04	0.1	0.2	0.03	0.1	0.01	0.2	0.04	LP12.CACB01A.C3.P2
Mixture	Calciocarbonatite, LREE	0.2	0.2	0.1	0.4	0.3	0.5	4	0.1	0.1	0.3	0.04	0.1	0.04	0.2	0.06	LP12.CACB01A.C4.P1
Mixture	Calciocarbonatite, LREE	0.2	0.2	0.1	0.3	0.1	0.4	5	0.1	0.2	0.2	0.02	0.2	0.03	0.2	0.03	LP12.CACB01A.C4.P1

the presence of REE minerals in fluid inclusions (Banks et al, 1994; Williams-Jones et al., 2012). Although very little data exist on the partitioning of REE between hydrothermal carbonate minerals and hydrothermal fluids, partition coefficient varying from 3980 for La (LREE) to 79 for Yb (HREE) has been calculated between calcite and sea water at 25 °C and 1 bar (Zhong and Mucci, 1995). This work suggests that REE can be expected to precipitate massively in carbonate minerals upon saturation and that LREE are expected to be further enriched over HREE during the precipitation process. These fluid/melt and mineral/fluid partitioning data clearly support the observation that REE at Montviel were concentrated in REE carbonates and fluorocarbonates via carbonic hydrothermal fluids (hereafter simply termed hydrothermal fluids), which exsolved from- and accompanied carbonatite melt. Alternatively, the hydrothermal fluid could have been generated simultaneously with the carbonatite melt, in the mantle or in the crust, in the presence or the absence of silicate magma.

4.3. LREE vs HREE zones

Zones of P and Ba hydrothermal precipitation were identified based on drill core assays during advanced exploration work and were sufficiently extensive to be shown on the scale of the carbonatite intrusion map (Fig. 3). These hydrothermal zones, as well as zones of Sr and F hydrothermal precipitation were recognized during hand sample and petrographic observations and correlated to specific mineral crystallization and REE-bearing mineralization (Section 3). The excellent correlation of total REE with Sr and the very good correlation of total REE with Ba for LREE zones (using Nd as a proxy for LREE) and the high Ba and Sr concentration only in LREE zones suggest that LREE mineralization was associated with Ba- and Sr-rich fluids. By contrast, only the HREE-rich zones are enriched in F and P, further suggesting that HREE mineralization was associated with F- and P-rich fluids. Given that the most HREE enriched mineral identified is ewaldite–(Y) and that it contains neither F nor P, F incorporated co-crystallizing minerals such as cordylite–(Ce) and fluorite and P formed co-crystallizing xenotime–(Y), monazite–(Ce) and apatite.

Given that LREE are more mobile than HREE (Wendlandt and Harrison, 1979; Samson and Wood, 2005; Williams-Jones et al, 2012), the simplest explanation for the existence of zones enriched in LREE is hydrothermal precipitation in ferrocarbonatite from Ba–Sr–LREE-bearing hydrothermal fluids. However, such differential transport capabilities between LREE and HREE cannot readily explain the existence of zones enriched in HREE. Given the association of HREE-rich zones with ewaldite–(Y) [$(Ba,Sr)(Ca,Na,Ln,Y)(CO_3)_2 \cdot nH_2O$], and high F and P drill core contents (Fig. 6c–d), we suggest that subsequent hydrothermal fluids with higher F and P contents must have transported more HREE and precipitated HREE-rich ewaldite–(Y) (in which HREE are more compatible), xenotime–(Y) (a HREE phosphate) and other fluorocarbonates

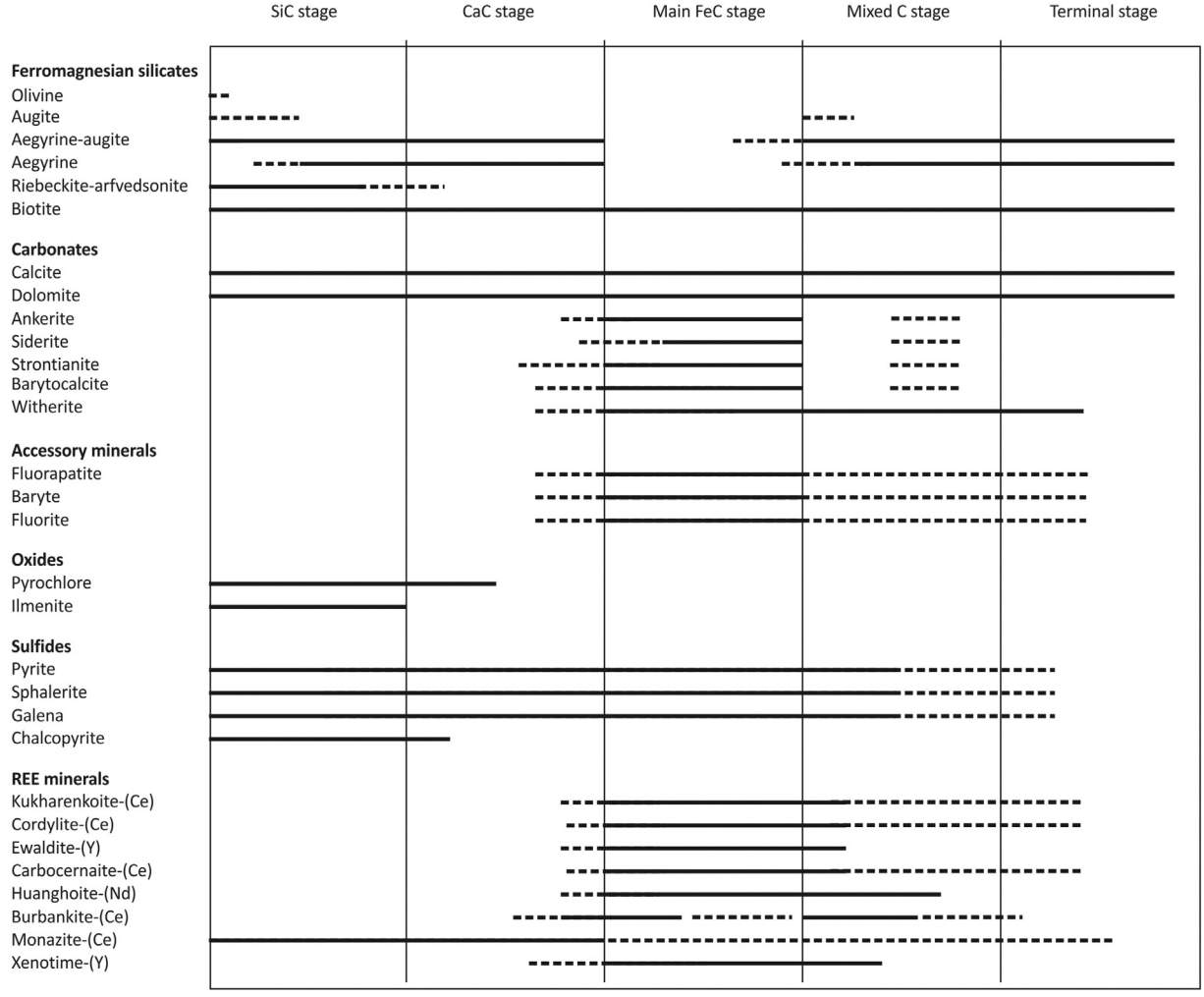

Fig. 11. Carbonatite mineral paragenesis. The Montviel carbonatite intrusion is divided in 5 stages that are simultaneously magmatic and hydrothermal: The silicocarbonatite (SiC) stage, the calciocarbonatite (CaC) stage, the ferrocarbonatite (FeC) stage, the mixed CaC–FeC–SiC stage and the terminal stage. Mineral is divided into ferromagnesian silicates, carbonates, accessory minerals, oxides, sulfides and REE-bearing carbonates, fluorocarbonates and phosphates. Bold lines represent the stages during which minerals crystallized but the exact timing of crystallization initiation or end is uncertain, as symbolized by dashed lines. Late, low temperature minerals such as quartz and hematite are not included.

such as cordylite–(Ce), huanghoite–(Nd) and kukharenkoite–(Ce). Preliminary results of $\delta^{18}O$ from carbonates in the polygenic breccia support the presence of lower temperature fluids circulating in- and possibly enriching the matrix of the breccia in HREE (Nadeau et al., 2013b).

4.4. Paragenetic model

Fig. 11 presents a magmatic–hydrothermal paragenetic sequence for Montviel based on the observations and analyses described above. The sequence defines the existence of a silicocarbonatite stage, a calciocarbonatite stage, a main ferrocarbonatite stage, a mixed SiC–CaC–FeC stage and a terminal stage. It should be noted that Montviel magmatic–hydrothermal system slightly resembles the four-stage model of Sokolov (1985) but differences between both systems are significant enough so that the Sokolov (1985) model is not used in this paper. At Montviel, all stages were initially dominated by magmas but all magmas were increasingly accompanied by magmatic volatile phases so that the system did not simply evolve from magmatic to hydrothermal, but instead was the locus of a continuum of alternating episodes of magmatic and hydrothermal activity. For example, the degree of hydrothermal alteration observed in silicocarbonatites (SiC) ranges from light to intense, and SiC magmatism–hydrothermalism was followed by calciocarbonatites (CaC), which are generally less altered than SiC. Ferrocarbonatites (FeC) following CaC – the main mineralization stage – vary from moderately to intensely hydrothermalized, with zones enriched in LREE ± Ba ± Sr and zones of HREE ± F ± P. Mixed SiC–CaC–FeC were subsequently injected in the magmatic–hydrothermal system, display light to moderate alteration and are generally fresher than other carbonatites but nevertheless host significant mineralization. The terminal stage was dominated by pressure buildup and explosion, creating the high-energy, funnel-shaped polygenic breccia (Nadeau et al., 2013a) which shows a matrix which is always strongly hydrothermally altered and often relatively enriched in HREE.

According to this paragenetic model, during the SiC stage, silicate magma coexisted with carbonatite magma and their magmatic volatile phases so that fresh, magmatic olivine was altered to ilmenite and carbonates (and serpentine, not shown in Fig. 11 for clarity). Augite was fenitized to aegirine–augite and aegirine. Magmatic and hydrothermal biotite was omnipresent. Magmatic calcite, dolomite, pyrochlore, ilmenite, pyrrhotite (not shown), sphalerite, galena, chalcopyrite, calcite, and monazite–(Ce) also crystallized.

During the CaC stage, magmatic Ca- and Mg-bearing carbonatite (calcite and dolomite) became preponderant but were still accompanied by significant concentrations of biotite, aegirine–augite and aegirine. Pyrochlore and monazite–(Ce) were still crystallizing from the carbonatite magma. Rare earth minerals which are non-equivocally magmatic could generally not be identified at that stage, except perhaps some euhedral and altered phenocrysts of burbankite–(Ce) (Fig. 9a), which are typically primary minerals in REE carbonatites (Chakhmouradian and Zaitsev, 2012). However, at some point during the CaC stage, Fe- CO_2-, Ba-, Sr-, F- and P-bearing magmatic fluids became more important and started crystallizing hydrothermal carbonates (ankerite, siderite, stontianite, barytocalcite, witherite), fluorapatite, barite, fluorite and Ba–Sr–REE carbonates and fluorocarbonates. This was the onset of the main, FeC stage, which was accompanied by a shift in the carbonatite towards more evolved, ferrocarbonatite compositions. Barium- and Sr-rich magmatic fluids repeatedly remobilized LREE and deposited LREE-bearing carbonates (burbankite–(Ce), carbocernaite–(Ce)) and fluorocarbonates (cordylite–(Ce), kukharenkoite–(Ce)) whereas relatively F- and P-rich fluids deposited more MREE to HREE mineralization (ewaldite–(Y), cordylite–(Ce), xenotime–(Y)), thus creating zones of LREE and HREE enrichments.

Subsequent injections of silicate and carbonatite magmas initiated the mixed, SiC–CaC–FeC stage, with renewed augite, aegirine–augite, aegirine crystallization and autometasomatism. Calcium- and Mg-dominated carbonatite took over other Fe–Ba–Sr-type carbonatite and lesser amounts of fluoroapatite, barite and fluorite crystallized. Nevertheless, REE carbonate and fluorocarbonate continued to precipitate from carbonatite magmatic hydrothermal fluids.

The terminal stage also appears to have been accompanied by renewed silicate and carbonatite magmatism with the crystallization of aegirine–augite, aegirine, calcite and dolomite. Nevertheless, this magmatic activity must have declined, as evidenced by preliminary results of $\delta^{18}O$ from carbonates in the polygenic breccia, suggesting that magmatic fluids were gradually contaminated by low temperature fluids (Nadeau et al., 2013b). The system must have sealed to some degree so that fluid pressure exceeded the confining, lithostatic pressure and a catastrophic rupture occurred, remobilizing the HREE and creating the HREE-enriched, funnel shape polygenic breccia pipe (Nadeau et al., 2013a).

Although the exact timing of periods of magmatic and hydrothermal activity and the extent to which they alternated remains unknown at Montviel, the paragenetic sequence generally indicates that hydrothermalism does not necessarily follow magmatic stages but that, instead, magmatism and hydrothermalism can be simultaneous and pulsatory. Repeated magmatic injections evolving towards hydrothermal end members resulted in a complex array of cross cutting magmatic and hydrothermal fingerprints. Montviel should thus been seen as an example of pulsatory magmatic–hydrothermal system, in contrast to more traditional unidirectional magmatic-to-hydrothermal systems.

Within this magmatic–hydrothermal system an immiscible BaFCl (±Si–O) melt appeared to have existed and contributed to the Ba and F hydrothermal precipitation and the REE mineralization process. This type of material is water soluble and ephemeral making its existence controversial, but has now been identified at Montviel and at Bayan Obo (Shimazaki et al, 2008).

5. Conclusions

The results and interpretations presented herein suggest the evolution of carbonatites whereby magmas and magmatic volatile phases evolved simultaneously via multiple injections of fluid-saturated carbonatite

Table 4
Major (wt.%) and trace element (ppm) content of the apatite-hosted, calciocarbonatite melt inclusion shown in Fig. 6f. Apatite was hosted in clinopyroxenite. Sample MV12.UM01.

Element	Concentration	1σ std. dev.	C normalized
CaO	54.9		
MgO	0.0		
FeO	0.1		
MnO	0.1		
SrO	0.9		
SiO_2	0.0		
CO_2	44.0		
Sr	1980	100	
Zr	0.35	0.03	
Nb	0.010	0.002	
Ba	23	18	
La	34.5	3.1	146
Ce	57.5	3.6	94
Pr	10.8	0.65	114
Nd	46.8	2.8	100
Sm	8.7	0.5	57
Eu	2.13	0.14	37
Gd	7.7	0.5	38
Tb	0.79	0.05	21
Dy	3.5	0.3	14
Y	11.3	0.9	7
Ho	0.53	0.04	9
Er	1.07	0.10	6
Tm	0.10	0.01	4
Yb	0.43	0.03	3
Lu	0.0475	0.0034	2
Hf	0.0024	0.0014	
Th	5.41	0.79	

magmas. A paragenetic sequence (Fig. 11) divides the evolution of the carbonatite into: (1) a silicocarbonatite stage which was initially magmatic but increasingly hydrothermal and which was the main Nb-mineralization stage; (2) a calciocarbonatite stage which was dominated by magma with very little hydrothermal fluids before the onset of; (3) ferrocarbonatite magmatism – the main mineralization stage – increasingly dominated by hydrothermal activity, periods of LREE ± Ba ± Sr hydrothermalism and periods of HREE ± F ± P hydrothermalism and resulting in the precipitation of burbankite–(Ce), carbocernaite–(Ce), ewaldite–(Y), huanghoite–(Nd), cordylite–(Ce), qaqarssukite–(Nd), kukharenkoite–(Ce), synchysite–(Ce) and other unidentified Ba–Sr–F carbonates, REE phosphates such as monazite–(Ce) and xenotime–(Y), fluorite and fluoroapatite; (4) renewed silicate–carbonatite activity resulting in a mixed SiC–CaC–FeC stage, which was followed by; (5) a terminal stage which resulted in catastrophic explosion, genesis of a HREE-rich polygenic breccia, cool down and death of the intrusive system.

More experimental work is required before differential REE transport capabilities are understood and zones enriched specifically in Nd, Dy and Y and mineral enriched in a variety of specific rare earth elements can be explained. This study underlines that despite their so-called similar geochemical behavior (Goldschmidt et al., 1925), REE do not necessarily behave homogeneously as a group and that individual LREE, MREE and HREE may be concentrated and separated by different processes. The present paper further demonstrates that rare earth elements should also be considered individually since specific minerals may be enriched or depleted in specific lanthanides, as demonstrated by the well-known Ce and Eu anomalies, and the Nd, Dy and Y anomalies present at Montviel.

The discovery of BaFCl (±Si–O) melt inclusions with heterogeneously trapped crystals of fluorite, and the existence of zhangpeishanite as inclusions in fluorite from Bayan Obo (Shimazaki et al., 2008) is important. The idea that such melt may contribute to carbonatite metasomatism and to REE mineralization is still in its infancy and future research should bear in mind that this possibility and the fact that such melts are ephemeral and water soluble.

Acknowledgments

This paper results from the financial contribution of Ressources Geomega and the collaboration of AC and MP from Ressources Geomega Inc. with ON, RS and MJ from UQAM/Geotop. NSERC grants 42576 to MJ and RS and FRQNT postdoctoral scholarship to ON all contributed financially to the present study. We thank Viorel Horoi and Thomas Barucchi for help with the GIS drawing. We also thank an anonymous reviewer and P. Downes for constructive reviews.

Appendix A. Supplementary data

Supplementary data to this article can be found online at http://dx.doi.org/10.1016/j.oregeorev.2014.12.017.

References

Banks, D.A., Yardley, B.W.D., Campbell, A.R., Jarvis, K.E., 1994. REE composition of an aqueous magmatic fluid; a fluid inclusion study from the Capitan Pluton, New Mexico, U.S.A. Chem. Geol. 113, 259–272.

Barker, A.L., 1975. Summary report on exploration work. Rapport statutaire déposé au ministère des Ressources Naturelles et de la Faune, Québec (GM 31071, 133 pp.).

Bell, K., Blenkinsop, J., Kwon, S.T., Tilton, G.R., Sage, R.P., 1987. Age and radiogenic isotopic systematics of the Borden carbonatite complex, Ontario, Canada. Can. J. Earth Sci. 24, 24–30.

Bühn, B., Rankin, A.H., 1999. Composition of natural, volatile-rich Na–Ca–REE–Sr carbonatitic fluids trapped in fluid inclusions. Geochim. Cosmochim. Acta 63, 3781–3797.

Chakhmouradian, A.R., Zaitsev, A.N., 2012. Rare earth mineralization in igneous rocks; sources and processes. Elements 8, 347–353.

Chao, E.C.T., Back, J.M., Minkin, J.A., Tatsumoto, M., Wang, J., Conrad, J.E., McKee, E.H., Hou, Z., Meng, Q., Huan, S., 1997. The Sedimentary Carbonate-hosted Giant Bayan Obo REE–Fe–Nb Ore Deposit of Inner Mongolia, China; a Cornerstone Example for Giant Polymetallic Ore Deposits of Hydrothermal Origin. U. S. Geological Survey, Reston, VA, United States, United States.

Corta, H., Berthelot, P., 2002. Rapport d'une campagne de sondages. Propriété Montviel. Ressources Nomans Inc., MRNF Val d'Or, Québec, rapport GM59647.

David, J., Dion, C., Goutier, J., Roy, P., Bandyayera, D., Legault, M., Rhéaume, P., 2006. Datations U–Pb effectuées dans la Sous-province de l'Abitibi à la suite des travaux de 2004–2005. Ministère des Ressources Naturelles du Québec, Rapport RP2006-04.

Desharnais, G., Duplessis, C., 2011. Montviel Core Zone REE Mineral Resource Estimate Technical Report, Quebec, Official 43-101 Ressouce Estimate (74 pp.).

Dimroth, E., 1970. Meimechites and carbonatites of the Castignon Lake Complex, New Quebec. Neues Jahrb. Petrol. Mineral. Abh. 112, 239–278.

Dumont, P., Sauvé, P., 1977. Rapport sur loes sondages 77-1 à 77-8, mars et juin 1977, propriété Montviel. Rapport statutaire déposé au ministère des Ressources Naturelles et de la Faune, Québec (GM 337667, 331 pp.).

Fleischer, M., Cabri, L.J., Chao, G.Y., Mandarino, J.A., Pabst, A., 1982. New mineral names. Am. Mineral. 67, 1074–1082.

Gauthier, M., Chartrand, F., Cayer, A., David, J., 2004. The Kwyjibo Cu–REE–U–Au–Mo–F property, Quebec; a Mesoproterozoic polymetallic iron oxide deposit in the northeastern Grenville Province. Econ. Geol. Bull. Soc. Econ. Geol. 99, 1177–1196.

Goldschmidt, V.M., Ulrich, F., Barth, T., 1925. Geochemische Verteilungsgesetze der Elemente: 4. Zur Krystallstruktur der Oxyde der seltenen Erdmetalle.

Goutier, J., 2005. Géologie de la région du lac au Goéland (32F15). Ministères des Ressources Naturelles et de la Faune, Rapport 2005-05 (39 pp.).

Goutier, J., Lalonde, A.E., 2006a. L'intrusion alcaline de Montviel, une premiere expression de magmatisme alcalin paleoprotozoique en Abitibi, Quebec. The Montviel alkalic intrusion, a first expression of Paleoproterozoic alkalic magmatism in Abitibi. Ministère des Ressources Naturelles du Québec, 31, p. 59.

Goutier, J., Lalonde, A.E., 2006b. Les mineralisations de niobium, de terres rares, de phosphates et de zinc de l'intrusion alcaline de Montviel en Abitibi, Quebec. GAC-MAC 2006. Geological Association of Canada, p. 59.

Hedrick, J.B., Sinha, S.P., Kosynkin, V.D., 1997. Loparite, a rare-earth ore (Ce, Na, Sr, Ca)(Ti, Nb, Ta, Fe^{+3})O_3. J. Alloys Compd. 250, 467–470.

Jébrak, M., 2007. Hydrothermal breccias in vein-type ore deposits; a review of mechanisms, morphology and size distribution. Ore Geol. Rev. 12, 111–134.

Klemme, S., 2004. Evidence for fluoride melts in Earth's mantle formed by liquid immiscibility. Geology 32, 441–444.

Kynicky, J., Smith, M.P., Xu, C., 2012. Diversity of rare earth deposits; the key example of China. Elements 8, 361–367.

Le Bas, M.J., Keller, J., Kejie, T., Wall, F., Williams, C.T., Zhang, P., 1992. Carbonatite dykes at Bayan Obo, Inner Mongolia, China. Mineral. Petrol. 46, 195–228.

Long, K., V.G., B.S., Foley, N.K., Cordier, D., 2010. The Principal Rare Earth Element Deposits of the United States — A Summary of Domestic Deposits and a Global Perspective. USGS (104 pp.).

Mariano, A.N., 1989. Nature of economic mineralization in carbonatites and related rocks. In: Bell, K. (Ed.), Carbonatite Genesis and Evolution. Unwin Hyman, pp. 149–172.

Mariano, A.N., Mariano Jr., A., 2012. Rare earth mining and exploration in North America. Elements 8, 369–376.

Mitchell, R.H., 1996. Perovskites: a revised classification scheme for an important rare earth element host in alkaline rocks. In: Jones, A.P., Wall, F., Williams, C.T. (Eds.), Rare Earth Minerals, Chemistry, origin and ore deposits. Chapman & Hall, pp. 41–71.

Mulja, T., 2006. The mineralogy of samples from a rare-earth element prospect and a base-metal prospect for Niogold mining corporation. Niogold, Ministère des Ressources Naturelles et de la Faune, Québec (Rapport GM62438).

Nadeau, O., Cayer, Al, Pelletier, M., Séguin, D., Stevenson, R., Jébrak, M., 2013a. Pétrométallogenèse du système alcalin carbonatitique (REE–Nb) de Montviel, Abitibi. Ministère des Ressources Naturelles et de la Faune, Québec Mines 2013 conference, Québec, Canada.

Nadeau, O., Stevenson, R., Jébrak, M., 2013b. Petrosomatic evolution of Montviel alkaline system and rare earth carbonatites, Abitibi, Canada. Goldschmidt 2013, Florence, Italy.

Philpotts, J., Tatsumoto, M., Li, X., Wang, K., 1991. Some Nd and Sr isotopic systematics for the REE-enriched deposit at Bayan Obo, China. Chem. Geol. 90, 177–188.

Sage, R.P., 1988. Geology of carbonatite–alkalic rock complexes in Ontario. Cargill Township Carbonatite Complex, District of Cochrane. Ontario Geological Survey, Canada (92 pp.).

Samson, I.M., Wood, S.A., 2005. The rare earth elements: behaviour in hydrothermal fluids and concentration in hydrothermal mineral deposits, exclusive of alkaline settings. Short Course Notes — Geological Association of Canada 17 pp. 269–291.

Sheard, E.R., Williams-Jones, A.E., Heiligmann, M., Pederson, C., Trueman, D.L., 2012. Controls on the concentration of zirconium, niobium, and the rare earth elements in the Thor Lake rare metal deposit, Northwest Territories, Canada. Econ. Geol. Bull. Soc. Econ. Geol. 107, 81–104.

Shimazaki, H., Miyawaki, R., Yokoyama, K., Matsubara, S., Yang, Z., 2008. Zhangpeishanite, BaFCl, a new mineral in fluorite from Bayan Obo, Inner Mongolia, China. Eur. J. Mineral. 20, 1141–1144.

Sokolov, S.V., 1985. Carbonates in ultramafite, alkali-rock, and carbonatite intrusions. Geochem. Int. 22, 150–166.

Sun, S.S., McDonough, W.F., 1989. Chemical and isotopic systematics of oceanic basalts; implications for mantle composition and processes. In: Saunders, A.D. (Ed.), Magmatism in the Ocean Basins 42. Geological Society of London, United Kingdom, pp. 313–345.

Sun, J., Zhu, X., Chen, Y., Fang, N., 2013. Iron isotopic constraints on the genesis of Bayan Obo ore deposit, Inner Mongolia, China. Precambrian Res. 235, 88–106.

Tremblay, J., Girard, R., 2012. Étude pétrographique et minéralogique de 28 échantillons de sondage et analyses à la microsonde électronique sur des échantillons sélectionnés. Projet Montviel, unpublished. official 43-101 ressource estimate.

Vasyukova, O., Williams-Jones, A.E., 2013. The role of fluoride–silicate liquid immiscibility in REE ore genesis. Goldschmidt 2013, Florence, Italy.

Vasyukova, O., Williams-Jones, A.E., 2014. Fluoride-Silicate melt immiscibility and its role in REE ore formation: evidence from the strange lake rare metal deposit, Québec-Labrador. Canada. Geochim. Cosmochim. Acta 139, 110–130.
Veksler, I.V., 2005. Element enrichment and fractionation by magmatic aqueous fluids; experimental constraints on melt–fluid immiscibility and element partitioning. Short Course Notes — Geological Association of Canada 17 pp. 69–85.
Veksler, I.V., Dorfman, A.M., Kamenetsky, M., Dulski, P., Dingwell, D.B., 2005. Partitioning of lanthanides and Y between immiscible silicate and fluoride melts, fluorite and cryolite and the origin of the lanthanide tetrad effect in igneous rocks. Geochim. Cosmochim. Acta 69, 2847–2860.
Veksler, I.V., Dorfman, A.M., Dulski, P., Kamenetsky, V.S., Danyushevsky, L.V., Jeffries, T., Dingwell, D.B., 2012. Partitioning of elements between silicate melt and immiscible fluoride, chloride, carbonate, phosphate and sulfate melts, with implications to the origin of natrocarbonatite. Geochim. Cosmochim. Acta 79, 20–40.
Wall, F., Mariano, A.N., 1996. Rare earth minerals in carbonatites; a discussion centered on the Kangankunde Carbonatite, Malawi. Mineral. Soc. Ser. 7, 193–225.
Wall, F., Niku-Paavola, V.N., Storey, C., Mueller, A., Jeffries, T., 2008. Xenotime–(Y) from carbonatite dykes at Lofdal, Namibia; unusually low LREE/HREE ratio in carbonatite, and the first dating of xenotime–(Y) overgrowths on zircon. Can. Mineral. 46, 861–877.
Wendlandt, R.F., Harrison, W.J., 1979. Rare earth partitioning between immiscible carbonate and silicate liquids and CO_2 vapor: results and implications for the formation of light rare earth-enriched rocks. Contrib. Mineral. Petrol. 69, 409–419.
Williams, C.T., 1996. Analysis of rare earth minerals. Mineral. Soc. Ser. 7, 327–348.
Williams-Jones, A.E., Migdisov, A.A., Samson, I.M., 2012. Hydrothermal mobilisation of the rare earth elements; a tale of 'ceria' and 'yttria'. Elements 8, 355–360.
Woolley, A.R., Kempe, D.R.C., 1989. Carbonatites; nomenclature, average chemical compositions, and element distribution. Carbonatites; Genesis and Evolution. Unwin Hyman, London, United Kingdom, pp. 1–14.
Woolley, A.R., Kjarsgaard, B.A., 2008. Paragenetic types of carbonatites as indicated by the diversity and relative abundances of associated silicate rocks: evidence from a global database. Can. Mineral. 46, 741–752.
Wyllie, P.J., Jones, A.P., Deng, J., 1996. Rare earth elements in carbonate-rich melts from mantle to crust. Rare Earth Minerals, Chemistry, Origin and Ore Deposits.
Zhong, S., Mucci, A., 1995. Partitioning of rare earth elements (REEs) between calcite and seawater solutions at 25 °C and 1 atm, and high dissolved REE concentrations. Geochim. Cosmochim. Acta 59, 443–453.